EFFECTS OF SURFACE PROPERTIES ON ADHESION OF PROTEIN TO BIOMATERIALS

A Thesis

by

FANGZHOU FENG

Submitted to the Office of Graduate Studies of
Texas A&M University
in partial fulfillment of the requirements for the degree of

MASTER OF SCIENCE

August 2010

Major Subject: Mechanical Engineering

EFFECTS OF SURFACE PROPERTIES ON ADHESION OF PROTEIN TO BIOMATERIALS

A Thesis

by

FANGZHOU FENG

Submitted to the Office of Graduate Studies of
Texas A&M University
in partial fulfillment of the requirements for the degree of

MASTER OF SCIENCE

Approved by:

Chair of Committee,	Hong Liang
Committee Members,	Melissa A Grunlan
	Christian J. Schwartz
Head of Department,	Dennis O'Neal

August 2010

Major Subject: Mechanical Engineering

ABSTRACT

Effects of Surface Properties on Adhesion of Protein to Biomaterials. (August 2010)

Fangzhou Feng, B.S., Wuhan University of Technology

Chair of Advisory Committee: Dr. Hong Liang

This thesis research investigates the adhesion mechanisms of protein molecules to surfaces of biomaterials. New understanding in such adhesion mechanisms will lead to materials design and surface engineering in order to extend the lifespan of implants. The present research evaluates and analyzes the adhesive strength of proteins on pure High Density Polyethylene (HDPE), Single Wall Carbon Nanotube (SWCNT) enhanced HDPE composites, Ti-C:H coating and Ti6Al4V alloys (grade 2). The adhesive strength was studied through fluid shear stress and the interactions between the fluid and material surfaces. The adhesive strength of protein molecules was measured through the critical shear strength that resulted through the fluid shear stress. The effects of surface and material properties, such as roughness, topography, contact angle, surface conductivity, and concentration of carbon nanotubes on adhesion were analyzed. Research results showed that the surface roughness dominated the adhesion. Protein was sensitive to micro-scale surface roughness and especially favored the nano-porous surface feature. Results indicated that the unpurified SWCNTs influenced crystallization of HDPE and resulted in a nano-porous structure, which enhanced the adhesion of the protein onto a

surface. Titanium hydrocarbon coating on silicon substrate also had a porous topography which enhanced its adhesion with protein, making it superior to Ti6Al4V.

DEDICATION

This work is dedicated to my mother, grandparents, aunt and to all of my relatives and friends. Without their support and help, I could not have completed the thesis.

ACKNOWLEDGEMENTS

I want to give special thanks to Dr. Liang who served as the chair of my committee. She let me work on tmy topic of choice. Her detailed guidance, patient encouragement, and helpful comments led to the successful accomplishment of this thesis. I am also grateful for the my other two committee members, Dr. Grunlan and Dr. Schwartz. Their insightful comments and wise advice aided the writing of this thesis in innumerable ways.

Again I want to thank Aracely Rocha, my friend and teacher, for teaching me how to use a rheometer and other experimental instruments. She gave me suggestions and helped me to solve problems that I encountered during my research. David Huitink and Brady Barkley's help with Atomic Force Microscopy (AFM) scans was crucial for my research. The X-ray Diffraction (XRD) scan performed by Michael Cleveland helped me better understand the composition of my samples. Feng Gao helped me in editing my paper and gave me many suggestions about sample polishing. I want to thank Kevin Plumlee for his help with the optical profilometer as well as thesis editing. Sanjay Kalidindi from Dr. Ounaies' group fabricated enough samples for my tests. All of these people are owed my greatest appreciation. Other members in Dr. Liang, Dr. Schwartz, and Dr. Ounaies's group also contributed their time and effort to help me when needed. Thanks also go to Dr. Ounaies from Aerospace Engineering Department as well as Dr. Polcar for their samples which were very important to this research.

Finally, I give special thanks to my friends, Joon Park, Oliver, Huisung, Sukbae, Chao, Songsheng, Yue, Jianhong and Ang, who made my life at Texas A&M University very wonderful.

NOMENCLATURE

UHMWPE	Ultra High Molecular Weight Polyethylene
HDPE	High Density Polyethylene
SWCNT	Single Wall Carbon Nanotube
CNT	Carbon Nanotube
SF	Synovial Fluid
PECVD	Plasma Enhanced Chemical Vapour Deposition
HiPco	High Pressure CO Disproportionation Process
wt	Weight Percent
DI	Deionized Water
Rc	Critical Radius
L_{10}	Distance of 10mm Measured by Image-J
Ac	Area of Protein Disk Measured by Image-J
τ_{Rc}	Critical Shear Stress
τ_{Rmax}	Maximum Shear Stress
Re	Reynolds Number
δ	Boundary Layer Thickness
ω	Rotational Speed of Spindle
η	Viscosity of Fluid
ρ	Density of Fluid
H	Height of the Base of Water Drop

R	Radius of the Base of Water Drop
r	Radius of Spindle Disk
θ	Contact Angle
Φ	Porosity Ratio
A_V	Total Area of Pores
A_T	Total Surface Area

TABLE OF CONTENTS

Page

Page

LIST OF FIGURES

Page

Page

Page

LIST OF TABLES

Page

CHAPTER I

INTRODUCTION

In this chapter, a comprehensive review of prior literatures will be given. The background theory about shear stress test will be provided. Following is an introduction to the fluid shear method to study fluid-material interfaces leading to the quantitative evaluation of average adhesive strength of cells or proteins to a substrate.

1.1. Material for artificial joint

Ultra High Molecular Weight Polyethylene (UHMWPE) and HDPE have been intensely studied for artificial joints for nearly 40 years [1-3]. UHMWPE and HDPE have excellent lubricity, biocompatibility, wear resistance and excellent mechanical properties, which make them good materials for artificial joints [4-5]. Their properties can be further improved by modern composite technology. Enhancing wear resistance and strength will allow new artificial joints to serve longer. This will reduce patients' pain suffered from surgery of replacing failed artificial joint. A typical artificial joint is composed of several parts and is shown in Fig. 1.

This thesis follows the style of Biomaterials.

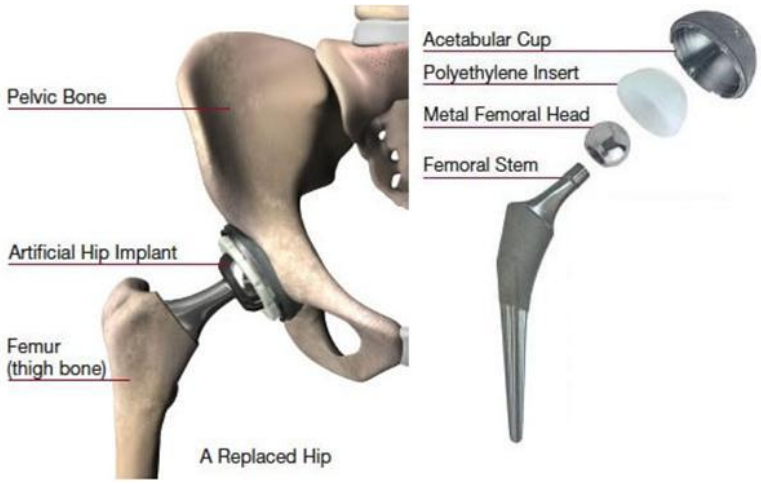

Fig. 1. Structure of a typical hip joint and its appearance after implant

The UHMWPE or HDPE coating on the metal femoral head is very important for artificial joint function. The polymer coating increases protein adsorption and improves the lubrication of the artificial joint [5-7]. Patient's activity, however, will wear the coating and release microscopic debris particles into the tissue around the joint. The accumulation of debris will cause tissue irritation and finally lead to osteolysis and to the loosening of the artificial joint components. Recent development indicated that incorporation of SWCNT enhanced strength and wear resistance of HDPE. This shows that such a material would be a good candidate for artificial joints [8-12].

1.2. Dental implant

Dental implants have special needs in biomaterials. Fig. 2 is a cross-section of a typical dental implant. Simply, it is a screw inserted into the jawbone. Once set, there are two interfaces with the implant. The first is between the implant surface and jawbone. This interface is important for the successful osseointegration process, which firmly anchors the dental implant into jawbone. The second interface is from the dental implant surface to the gum tissue. Ideally if the gum tissue attaches well to the dental implant surface it can serve as a protective barrier. In such, food debris will not enter to the root area and corrode the dental implant surface [13]. Corrosion may result in loosening and failure of the dental implant. Currently, the widely used material for dental implant is the titanium-alloy, Ti6Al4V [14-15]. This material is successful because of its outstanding mechanical and chemical properties. Moreover the TiO_2 film formed on the surface of Ti6Al4V increases its wear resistance and hardness. TiO_2 can aid in the successful osseointegration and form a good interface with oral soft tissue [16-17].

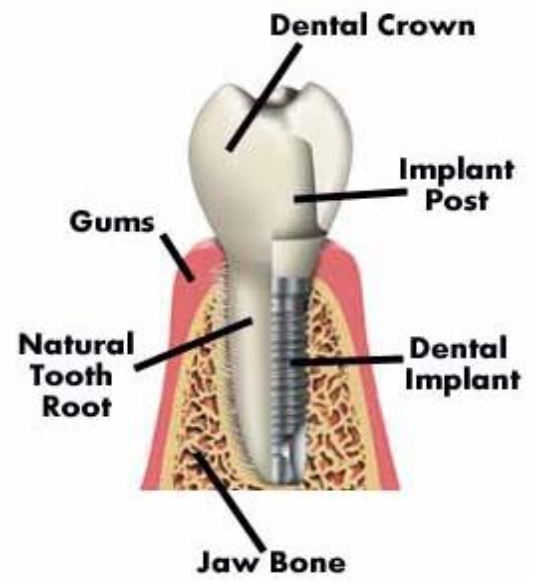

Fig. 2. Structure of a dental implant

It has been found that Ti-C:H has superior properties than titanium oxide as a coating [18-21]. Whether it could be used for dental implant coating needs to be investigated. To meet these demands, Ti-C:H needs to have a good interface with gum tissue. The first step for the formation of that interface is protein adhesion, followed by cell adhesion. Shear stress tests can test the adhesive strength of albumen to titanium hydrocarbon coating on a silicon substrate and Ti6Al4V. Comparison of these results will allow the selection of the best material.

1.3. Current issue in artificial joints

New materials for artificial joints have always been a driving force for the development of orthopedic implants. Recently in worldwide, each year more than 800,000 hip joints are replaced and over 500,000 knee replacement surgeries enable patients to walk without pain [22-23]. This trend is true for the world, most notably in China, Japan, and Germany. The reason is that the baby boomers after World War II are now aging and experiencing a variety of health problems, including the deterioration of their skeletal systems [1].

1.4. Cell-materials adhesion

Cell and protein adhesion on different bio-materials is one of the most important aspects for an implant device [24-26]. When a foreign material enters into our body and contacts body tissue or bio-fluid, protein adsorption occurs[24, 27]. Without the protein adsorption, cells cannot attach on the implant surface and form a good interface with the implant.

Cell adhesion are influenced by surface roughness in macro-scale (around 0.60μm). Moreover proteins are sensitive to surface topography in the nanometer scale (1-4nm) [28]. Deligianni [29] reported that human bone cells could detect the surface roughness in the order of 0.60μm. In the same report, a high surface roughness benefited cell

adhesion and proliferation. Galli [28] reported that micrometer scale topography could influence protein adhesive strength to a surface. In other reports, methodology had been developed to quantify the adhesion of albumen on the substrate [30-32]. A summary of various studies of cell adhesion is listed in Table 1. Questions arose regarding effects of surface properties on cell adhesion in terms of interfaces of fluid, cell, and bio-molecules [33-36].

Table 1 Summary of cell and protein adhesion study on different substrates

Year	*Author*	*Test Summary*	*Results*
2001 [37]	*Deligianni*	*Human bone cell adhesion on hydroxyapatite*	*Surface roughness affects cellular response, enhancing cell adhesion and proliferation*
2001 [29]	*Deligianni*	*Bone marrow cell, bovine serum albumin and fibronectin coated on Ti6Al4V*	*Serum albumin adheres better to the smoother substratum. Cell adhesion and proliferation can sense surface roughness*
2002 [28]	*Galli*	*Protein A, IgG and F-actin on Si and Ti surfaces with different topography*	*Surface topography in nanometer scale can influence protein adhesive strength*
2004 [4]	*Heuberger*	*Human serum albumin (HAS) on UHMWPE*	*More hydrophilic surfaces preferentially adsorb protein of native conformation*
2009 [30]	*Rocha*	*Shear stress analysis for cell adhesion on polymer substrate*	*A method was developed to quantify cell adhesive strength to materials*
2010 [31]	*Fritsche*	*Osteoblastic cells on Ti6Al4V, Co28Cr6Mo and 316L*	*Prove spinning disc shear stress test can be used for quantifying bone cell adhesive strength to biomaterials of orthopedic implants*

CHAPTER II

MOTIVATION AND OBJECTIVES

The current materials for artificial joint and dental implant do not satisfy the requirement due to lack of protein adhesion. So this research aims to obtain basic understanding of adhesive mechanisms. This will help improve the protein adhesion and subsequently the service life of artificial joint and dental implant. There are two objectives in the present research.

1. Obtain fundamental understanding in molecular interactions between protein molecules and biomaterials. Such understanding can be firstly obtained through experimental and quantitative evaluation of adhesive strengths through fluid shear.
2. Develop knowledge in surface properties on protein adhesion. The surface features include roughness of a surface, topography, contact angle and conductivity of a surface.

The primary approach is to carry out fluidic experiments using a rheometer. The same type of proteins will be tested and SWCNT-HDPE composites and Ti-C:H coating will be studied.

CHAPTER III

EXPERIMENT PROCEDURES

In this chapter the experimental procedure will be provided. Information about materials tested will be discussed. Fluid shear stress experiments will be conducted in laminar flow condition which is critical for adhesion study.

3.1. SWCNT-HDPE sample preparation

Pure HDPE sample films were prepared using the following method. HDPE pellets and o-xylene liquid (Sigma Aldrich) were used for this study. Firstly HDPE pellets (1.5g) and o-xylene (9.5g) were placed into a beaker on a hot plate and heated to 150℃ , and stirred at 300rpm using a magnetic stirrer. After the HDPE pellets dissolved completely, the HDPE/o-xylene solution was poured onto a heat-resistant ceramic plate that was pre-heated to 150ºC. A doctor blade moved across to create film of uniform thickness (40μm).

Purified SWCNT-HDPE nanocomposites were produced using the following method provided by collaborators. SWCNTs were fabricated by high pressure CO disproportionation process (HiPco) [38-39]. Raw SWCNTs were purified with nitric acid reflux and gas phase oxidization process. The SWCNTs were dispersed in o-xylene for two hours using probe sonication at 25 Watts power. The solution was then heated to

150°C and mixed with a HDPE/o-xylene hot solution on a stirring hot plate. HDPE/o-xylene solution used was the same as that prepared for pure HDPE samples. The stirring process involved magnetic stirring at 300 rpm for three hours followed by six hours of probe sonication process. The casting process for the SWCNT-HDPE composites was the same as pure HDPE. Unpurified SWCNT-HDPE composites were also prepared in order to compare with purified SWCNT-HDPE samples. For the unpurified SWCNT-HDPE composites raw SWCNTs was directly used without any purification process.

After solution casting, samples were stored in a desiccator until they solidified. Samples were put into a vacuum oven at 80ºC in order to eliminate any remaining o-xylene in the film. The solution casting process produces was used to make samples into different surface roughness on either side. The bottom surface was generally smoother than the top (shown in Fig. 3). Both sides of sample were evaluated in order to eliminate chemical composition difference and only investigate how surface features influence albumen adhesion.

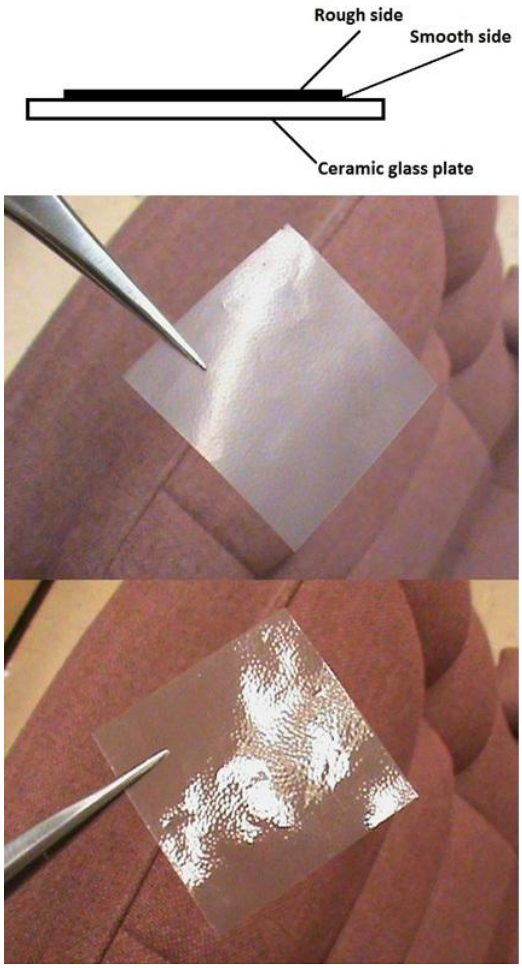

Fig. 3. Top (up) and bottom (down) surface of a sample film

The sample film was set on a glass slide to obtain a flat surface. The sample film was cut into 25 x 25 mm^2 pieces. They were then secured on a microscope slide with a high strength medical grade double-sided tape (shown in Fig. 4). Care was taken to avoid trapped air between layers. The samples were cleaned with DI (deionized) water and allowed to air dry in individual petri-dishes to prevent further contamination. Twelve samples were prepared for each weight percent SWCNTs composites and for

both top and bottom surface: 0.1 %, 0.2 %, 0.5 % unpurified, and 2.5 %wt separately. Pure HDPE samples were used as a control.

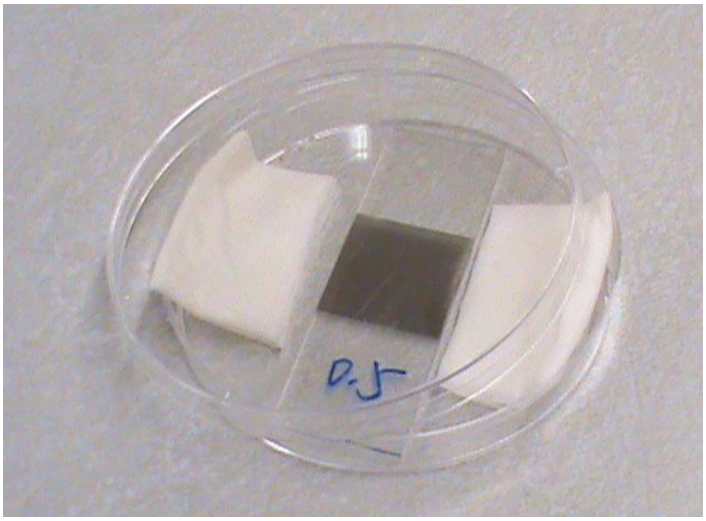

Fig. 4. Structure of sample

The sample surface was then coated with albumen solution. The 2.91 %wt albumen solution was prepared by mixing 0.300±0.005g albumen powder into 10ml DI water. It was stirred for 20min using a magnetic stirrer. The amount of 100µl of albumen solution was coated on the surface of each SWCNT-HDPE composite sample using a pipette. In cases of inconsistent humidity, the protein coating would crack and/or peel off the surface prior to testing. To prevent this, each sample, along with two DI water saturated facial tissues, was paced into a partially covered petri-dish and allowed to air dry for 12 hours (shown in Fig. 5). Six samples with the same SWCNTs concentration were prepared as a group for each test.

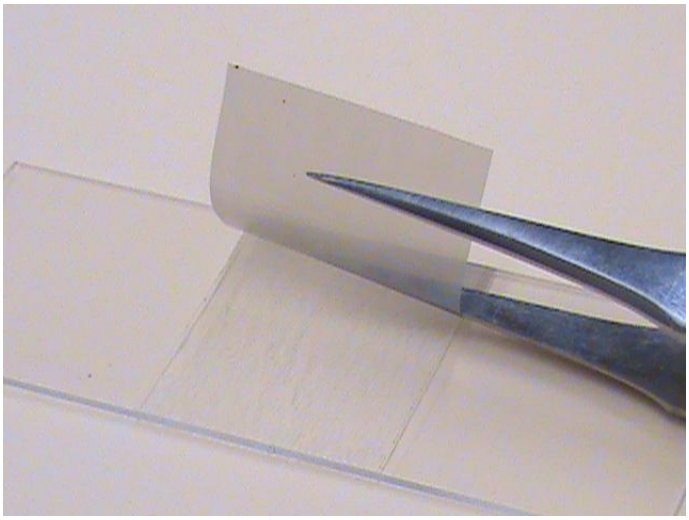

Fig. 5. Humidity controlled setting

3.2. Materials

Since SWCNTs-enhanced-HDPE is for artificial joint coating, the experiment is designed to imitate the behavior of artificial joints once implanted into the body. Rheometer has been used to carry out the shear stress experiments because it is similar to the working conditions of artificial joints. Artificial joints are actually a ball-cup bearing system, while the rheometer is a rotating and stationary disk system. The rotating disk comparable to the femoral head of artificial joint and the stationary disk is similar to the acetabular cup positioned in the pelvic bone. In this research water is used to imitate the bio-fluid in the body.

Egg white protein (albumen) is coated on the sample surface to imitate the protein adhesion on the surface in an artificial joint or dental implant. When the surface of a foreign material contacts a bio-fluid or body tissue, protein adsorption takes place. Then cells start to grow on that layer of protein. Finally, the body forms an interface with the material [24]. Without protein adsorption, cell adhesion cannot begin and body will reject the implants. Second synovial fluid (SF), which is the natural lubricant for human's articular joints, is composed of lipids, hyaluronic acid (HA) and lubricin. Lubricin is a water-soluble glycoprotein and it plays a very important role in joint lubrication. Egg white protein contains 54 % Ovalbumin and 12 % Ovotransferrin, both glycoproteins [40-41]. Furthermore collagen fibers, proteoglycan and elastin fibers are major components of cartilage (shown in Fig. 6). All of these three components are protein similar to albumen without exception. Therefore it is valid to use it in this study.

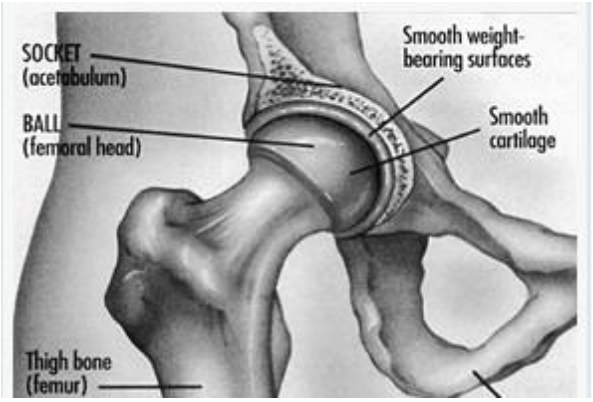

Fig. 6. Cartilage in human hip joint

Overall using a rheometer, the combination of water and egg white albumen is a good simulation of the working conditions of artificial joints.

3.3. Fluid shear stress measurement

We have recently developed a methodology to analyze the average adhesive strength of a cell or protein on to a substrate involving well defined shear stress[30]. This method employs a parallel plate rheometer (shown in Fig. 7) to quantify protein or cell adhesive strength on a material. During the experiment a round plate or spindle rotates over the sample and applies a shear stress on the protein through the fluid between the sample and the spindle. A laminar flow condition is required for the shear stress analysis. In this test the Reynolds number was less than 2.9×10^4 by using the following equation.

$$Re = \rho\omega r^2/\eta \quad (1)\ [30, 42]$$

where ω is the rotational speed, r is the radius of the spindle disk, and η and ρ are the viscosity and density of fluid. The radius to boundary layer thickness ratio, calculated from the spindle radius divided by the boundary layer thickness, was 30.49. The boundary layer thickness, δ, is calculated from the following equation.

$$\delta = 5.5(\eta/(\rho\omega))^{1/2} \quad (2)$$

According to H. Schlichting and K. Gersten [31, 43-45] the laminar flow condition and the assumption of an infinitely large disc are satisfied. Laminar flow condition can simplify the calculation processwhile an infinitely large disc assumption is used to eliminate the turbulent flow near the rim of the spindle.

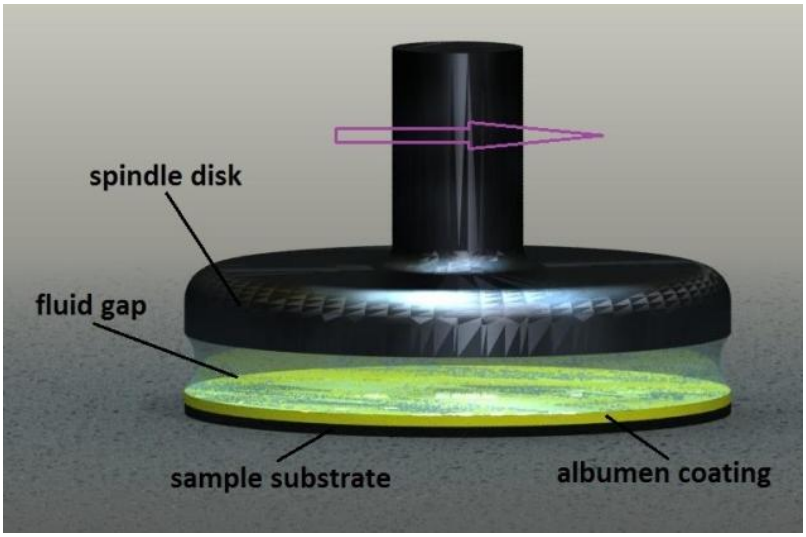

Fig. 7. Rheometer system

Since the flow is laminar, the radial position or critical radius (Rc) on the sample and the applied shear stress or critical shear stress (τ_{Rc}) at that location has a linear relationship. The maximum shear stress (τ_{Rmax}) on the rim the disk is controlled by the rheometer. So if the distance between this point and the center (Rc) are measured, the following equation can calculate the critical shear stress (τ_{Rc}).

$$\tau_{Rc} = \tau_{Rmax} \frac{Rc}{r} \qquad (3)$$

where r is the radius of the disk (shown in Fig. 8).

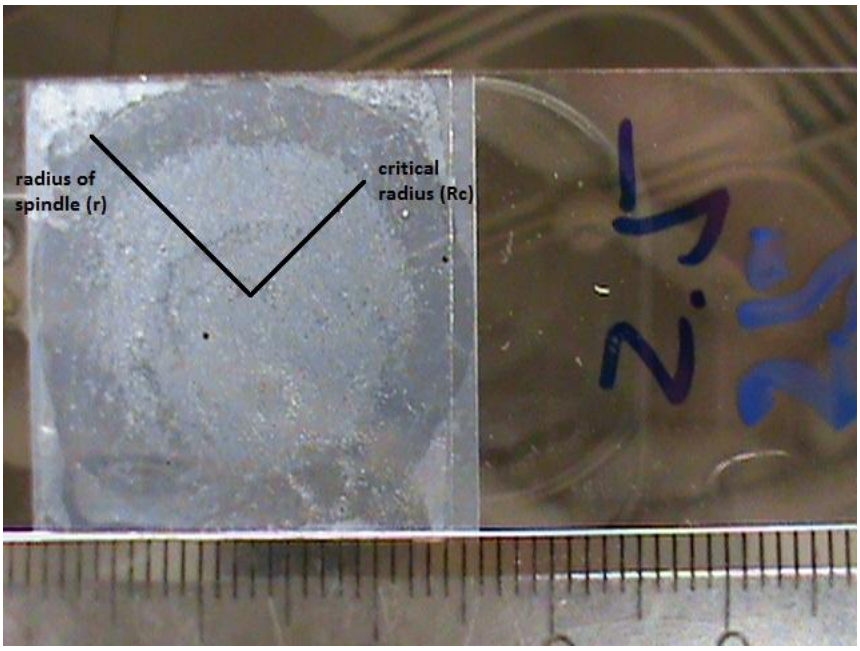

Fig. 8. Tested sample shown critical radius (Rc)

Before experiments the sample surface was coated with albumen. During the test the proteins close to the rim of the spindle were removed because the applied shear stress

was highest. As the radius decreased the applied shear stress also decreased. This led to a point on the surface (the critical radius) at which the albumen remained on the surface. This was due to the applied shear stress at this point not sufficient enough to overcome the albumen adhesive strength to the sample. Albumen coating on a sample surface after testing showed a disk shape protein distribution (Fig. 9). Then we measured Rc and used it in equation (3) to calculate the τ_{Rc}. This τ_{Rc} represented the adhesive strength between the sample and albumen.

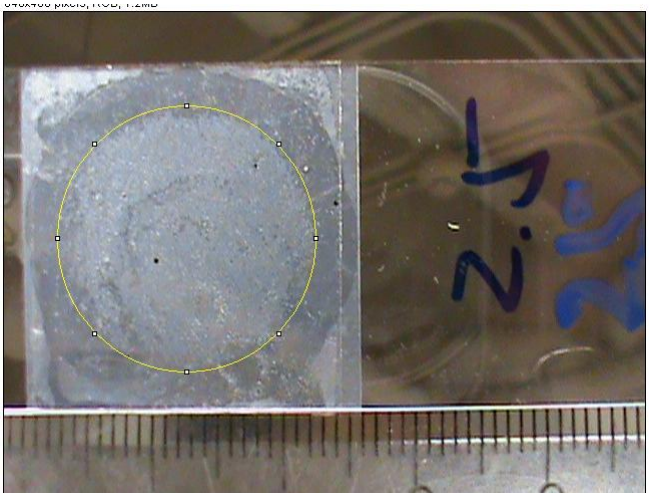

Fig. 9. Measuring the critical radius (Rc)

Image analysis is used to measure the critical radius of the albumen left on the sample. The software Image-J allows for the measurement of distances in pixels. Firstly, the number of pixels was counted along a 10mm (L_{10}) ruler that was placed next to the sample. Secondly, the area of the protein (Ac) left on the sample after testing was measured using a circle (shown in Fig. 9). Finally, the critical radius (Rc) of the sample was obtained by using the following conversion.

$$R_c = \frac{10}{L_{10}} \cdot \sqrt{\frac{Ac}{\pi}} \qquad (4)$$

Critical shear stress will be used to quantify the adhesion of albumen to the sample surface. Standard error will be used to calculate the length of the error bar.

3.4. Shear stress test procedure

The AR-G2 Rheometer (TA Instruments) was used to carry out experiments by controlling maximum shear stress applied on the sample (shown in Fig. 10). The rotating disk was a 25mm diameter spindle while the sample was fixed on the stationary disk below.

Fig. 10. AR-G2 rheometer
Courtesy of TA Instrument

The stationary plate is a peltier plate for temperature control. The temperature was maintained at 25 ^{o}C. The amount of 200±1µl of DI water was poured on the sample to fill the 500µm gap between the spindle and the sample (shown in Fig. 11). When lowering the spindle, it rotated at a low speed in order to form an evenly distributed water layer without air bubbles (shown in Fig. 12). Each shear stress test took for 5min. Shear strain, spindle speed, torque and temperature were recorded. Immediately after testing, protein distribution on sample surface was recorded using a digital camera for image analysis (Image-J). Six samples in one group were exposed to different controlled shear stress, namely 25, 26.5, 28, 29.5, 31 and 32.5Pa.

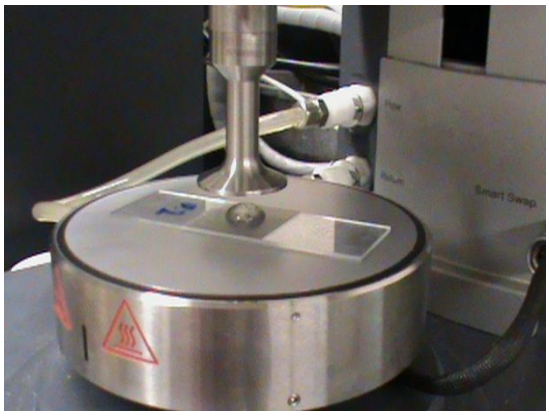

Fig. 11. DI water dropped on sample surface

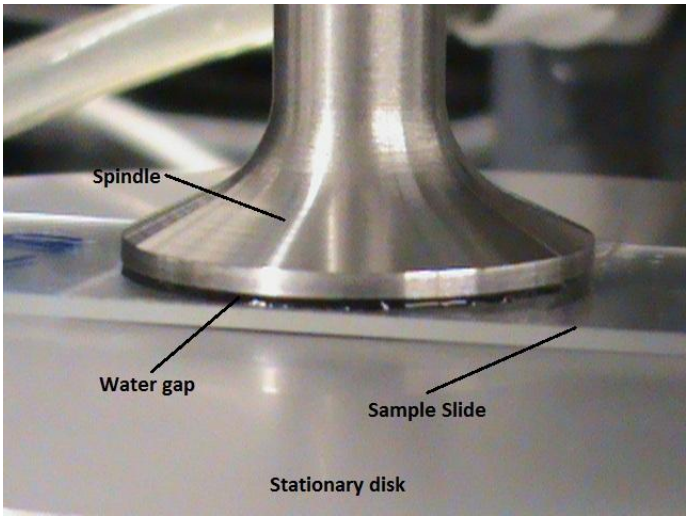

Fig. 12. View of test procedure

Samples were cleaned with distilled water after each test to remove all proteins from the surface and allowed to air dry before being recoated with albumen and retested. To improve accuracy and repeatability, each test was repeated for three times.

3.5. Surface roughness test

The macro-scale surface roughness of all samples, 0.1, 0.2, 0.5 unpurified, 2.5 %wt SWCNT-HDPE, pure HDPE, Ti-C:H coating and Ti6Al4V was measured respectively with a profilometer (Zygo newview 600s optical) in 0.14mm x 0.11mm scale (shown in Fig. 13). An optical profilometer uses a non-contact mode to measure surface roughness and its profile. The average value for each group was used to

represent its macro-scale surface roughness. The macro-scale surface roughness and surface profile have been reported to show effects on cell adhesion [29]. The present research focuses on protein adhesion.

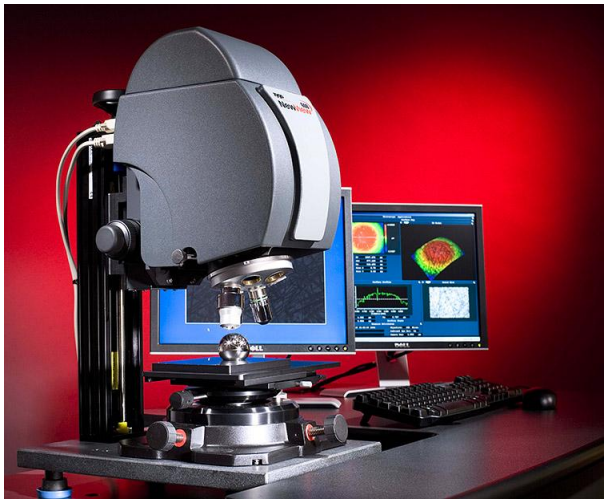

Fig. 13. Optical profilometer
Courtesy of Zygo

3.6. Contact angle measurement

Contact angle was tested in the following method. The amount of 0.05ml distilled water was dropped onto the sample surface from a 5mm height. Once the drop was on the surface, a digital camera was used to take an image. The height (h) and radius (r) of the base of the drop were measured with Image-J (shown in Fig. 14). The equation (5) below was used to calculate the contact angle (θ).

$$\tan\left(\frac{\theta}{2}\right) = H/R \qquad (5)$$

Contact angle test is necessary because protein had some preference to hydrophilic surface [4]. Doing so enabled us to study how the contact angle affects the adhesion of protein to a surface.

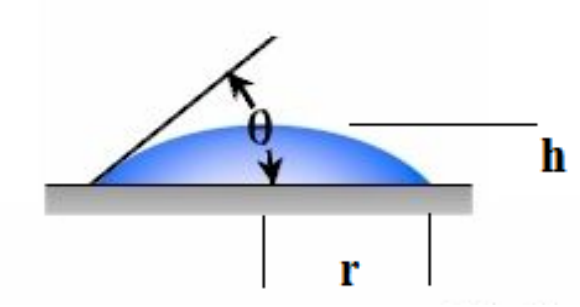

Fig. 14. Contact angle of albumen solution on sample surface

3.7. AFM imaging analysis

An AFM (Pacific Nanotechnology, Inc.) was operated with close-contact mode to scan the surface of each sample (shown in Fig. 15). Scan sizes of 5μm x 5μm were obtained using a silicon cantilever with scan rates of 1Hz and a resolution of 256x256 pixels. Images were analyzed by NanoRule to obtain the surface roughness on the micrometer scale.

Nano-scale surface roughness and topography were evaluted in order to compare the same with macro-scale surface roughness and topography.

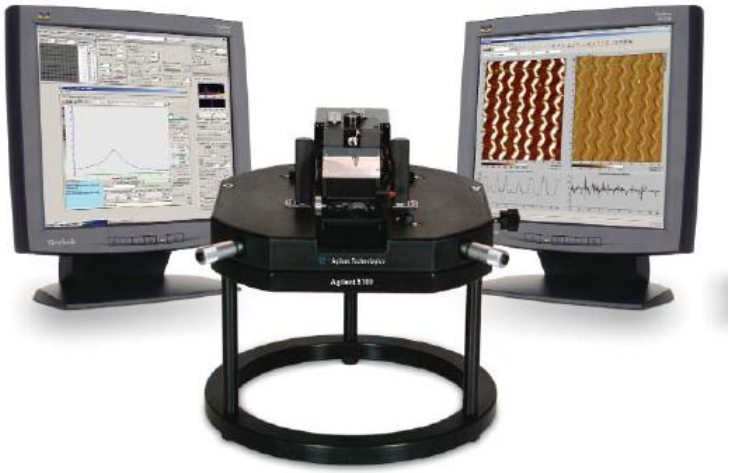

Fig. 15. AFM
Courtesy of Pacific Nanotechnology Inc.

3.8. Surface conductivity test

The surface conductivity was tested using the simple “2-probe technique”. Two test probes of a digital multimeter (shown in Fig. 16) touched the sample with one centimeter apart. Electric conductance was read directly from the mulitmeter. The unit of the surface conductance was nS/cm (nano-siemens per centimeter). Every sample surface was tested for five times and the average was reported.

Since protein is a highly negative charge molecule, the surface conductivity was to evalute the electronegantivity in the compostie sample. The hypothesis was based on the fact that one of the sample groups was fabricated from unpurified SWCNTs. The unpurities in those SWCNTs were mainly iron particles.

Fig. 16. Digital multimeter

3.9. XRD scan

Data collection range was from 5 degree to 70 degree (Fig. 17). Data was analyzed by using the program EVA.

XRD scan was used to investigate the chemical composition and/or crystallographic structures.

Fig. 17. XRD (Bruker D-8 Bragg)
Courtesy of Bruker Corp.

3.10. Ti-C:H coating and Ti6Al4V sample preparation

Titanium hydrocarbon coating was fabricated using PECVD (plasma enhanced chemical vapor deposition) process with acetylene (C_2H_2) as a reactive gas. Ti was sputtered on a silicon substrate by magnetron sputtering in an argon atmosphere. The final chemical composition of the coating was 19 % mol of Ti and 81 % mol of C was

achieved by controlling the acetylene flow rate to 45sccm during the deposition process. The sample was set on a glass slide similar to the SWCNT-HDPE composite films (shown in Fig. 18). The protein coating procedure for these samples were the same as SWCNT-HDPE composites.

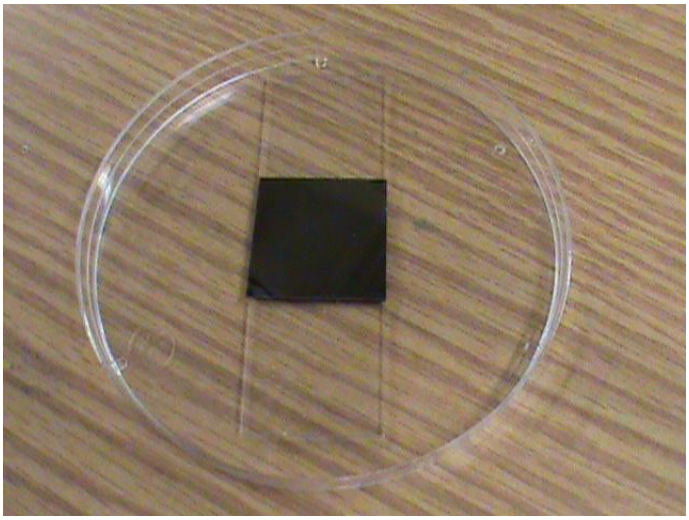

Fig. 18. Ti-C:H coating on silicon substrate sample settled on glass slide

Ti6Al4V grade 2 (McMaster-Carr) was polished with grinding papers. To make the titanium-alloy surface having a similar surface roughness as the Ti-C:H coating, the Ti-alloy were cut into 28mm x 28mm pieces and polished by three types of grinding papers (shown in Fig. 19). Samples were polished by usng the Polisher Ecomet Π Grinder (Buehler Ltd.) Tap water was used as the lubricant. Samples were firstly polished by a 400-grit silicon carbide grinding paper (Buehler Ltd.), followed by a 600 grit grinding paper (High Tech Products Inc.). Finally the sample surface was finished

by an 800 grit grinding paper. The optical profilometer scans show that the titanium-alloy sample surface polished by this procedure has a macro scale surface roughness similar to the Ti-C:H coating.

Fig. 19. Ti6Al4V (grade 2)

CHAPTER IV

FLUID AND SURFACE PROPERTIES

This chapter describes experimental results in terms of surface physical and morphological properties. Those include macro and micro scale surface roughness, surface topography, contact angle, surface conductivity and XRD scan.

4.1. Macro scale surface roughness test result

The micrometer length scale surface roughness from the optical profilometer are shown in Fig. 20. There are two points here. The first is that the top surface of each sample has higher macro scale surface roughness than the bottom surface. The second finding is that the pure HDPE has higher macro scale surface roughness than the composite samples for both top and bottom surface. For the Ti-C:H and Ti6Al4V samples, their macro scale surface roughness are similar.

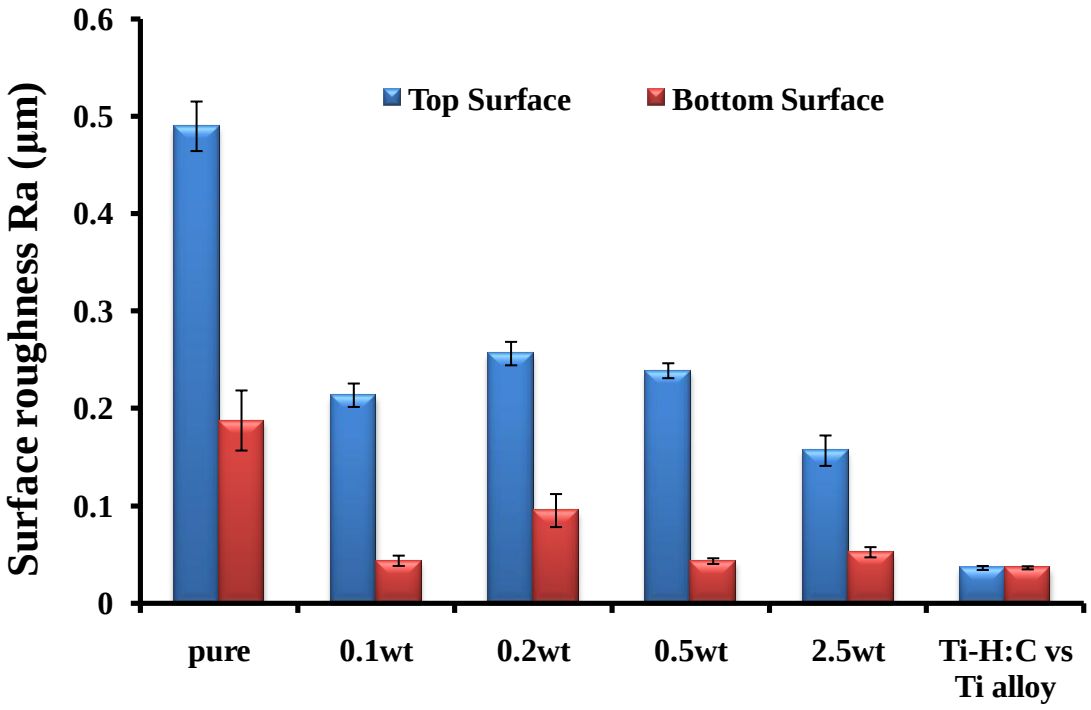

Fig. 20. Surface roughness (macro scale) of top and bottom surface for each sample group

4.2. Contact angle test result

The contact angle results (Fig. 21) show that the bottom surface of every sample has a higher contact angle than the top surface. Furthermore Ti-C:H coating is more hydrophobic than Ti-alloy. This means that Ti-alloy surface more preferentially adsorbs protein than Ti-C:H coating.

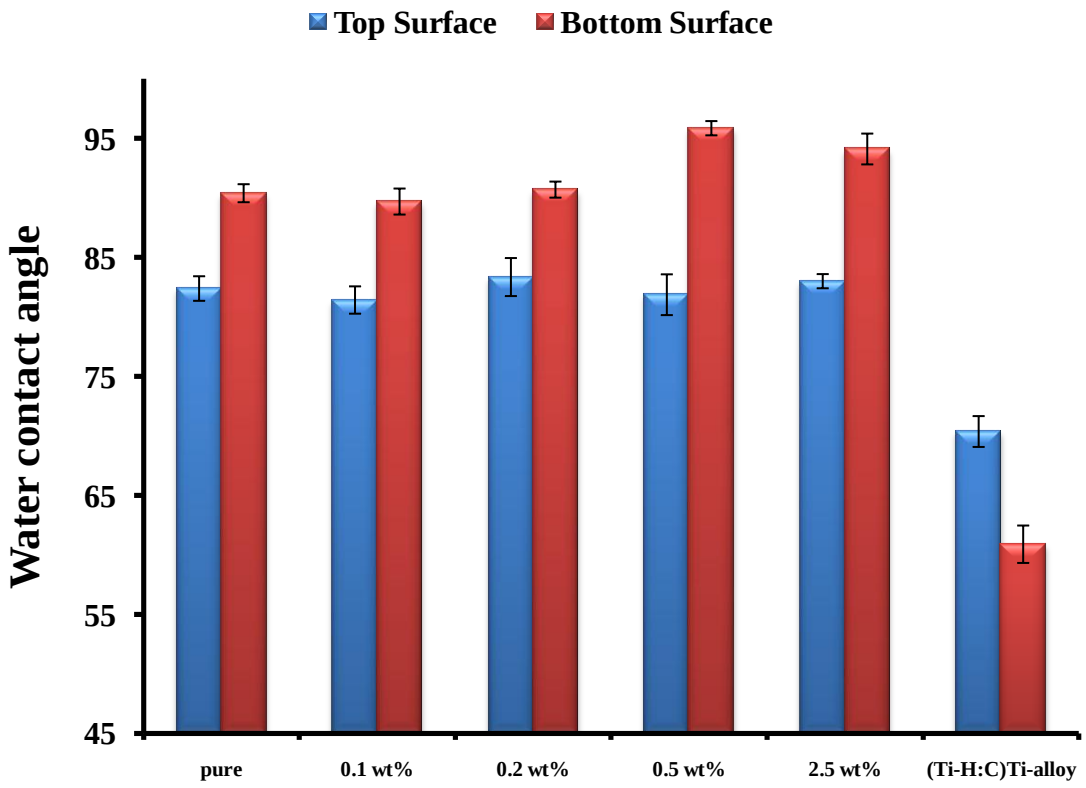

Fig. 21. Contact angle of top and bottom surface for each sample group

4.3. Surface conductivity test result

The surface conductivity test results (Fig. 22) indicate that the surface conductivity for the two surfaces of each sample is similar. The 0.5 %wt unpurified SWCNT-HDPE composite sample has much higher surface conductivity than other groups. The impurities in the SWCNTs are mainly iron particles which were introduced during the fabrication process. Iron particles are significantly more conductive than HDPE. That is why the unpurified composite sample groups have a higher surface conductivity than others.

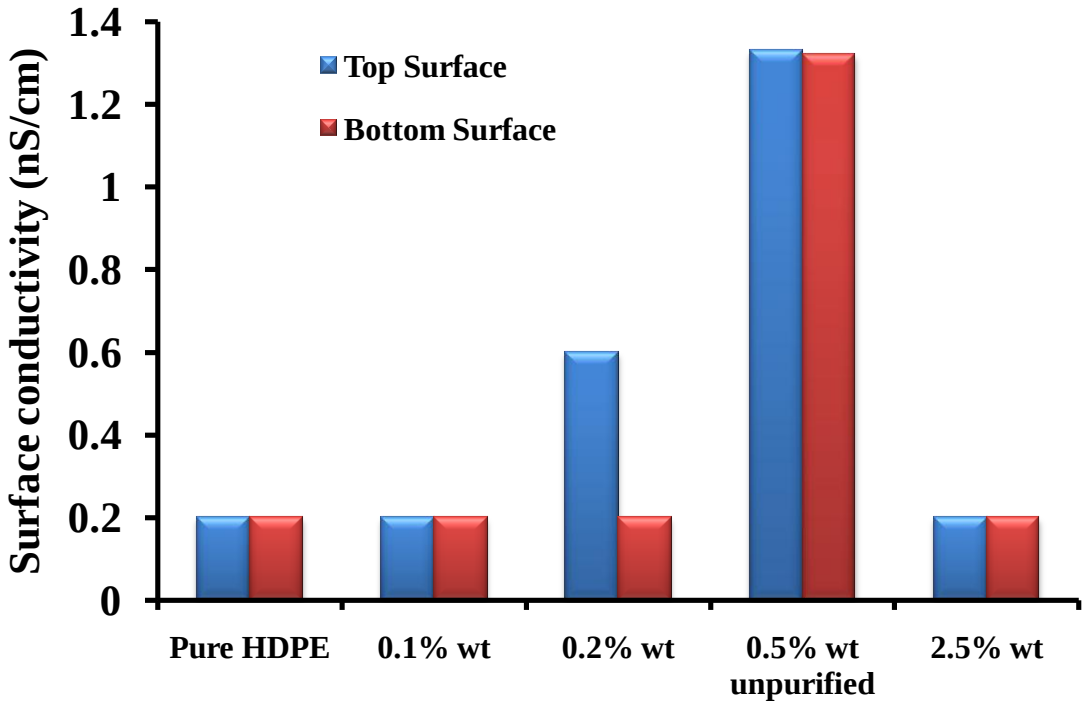

Fig. 22. Surface conductivity for top and bottom surface

4.4. Shear stress test results

The shear analysis results are summarized in Fig. 23, Fig. 24 and Fig. 25. The error bar is the standard error of data group. In Fig. 25 each sample group may be identified with a different trend line color. A dash line is used to identify the top surface while the solid line is used for the bottom surface. According to the figures, for a sample with a specific weight percent of SWCNTs, the top surface does not always have better adhesion with albumen than its bottom surface.

In addition the adhesion results for the bottom surface of all samples have a similar adhesion force with albumen. Their trend lines (shown in Fig. 24) generally overlap. The adhesion results for the top surface show a significant difference as noted by the obvious shift of their trend lines (shown in Fig. 23).

Finally the top surface of 0.5 %wt unpurified SWCNTs/HDPE has the strongest adhesive strength with albumen than all of the others. The top surface of pure HDPE, which performs as control, shows strong adhesion with albumen following the top surface of 0.5 %wt unpurified SWCNTs/HDPE.

Ti-C:H coating on silicon substrate has higher adhesive strength with protein than Ti6Al4V.

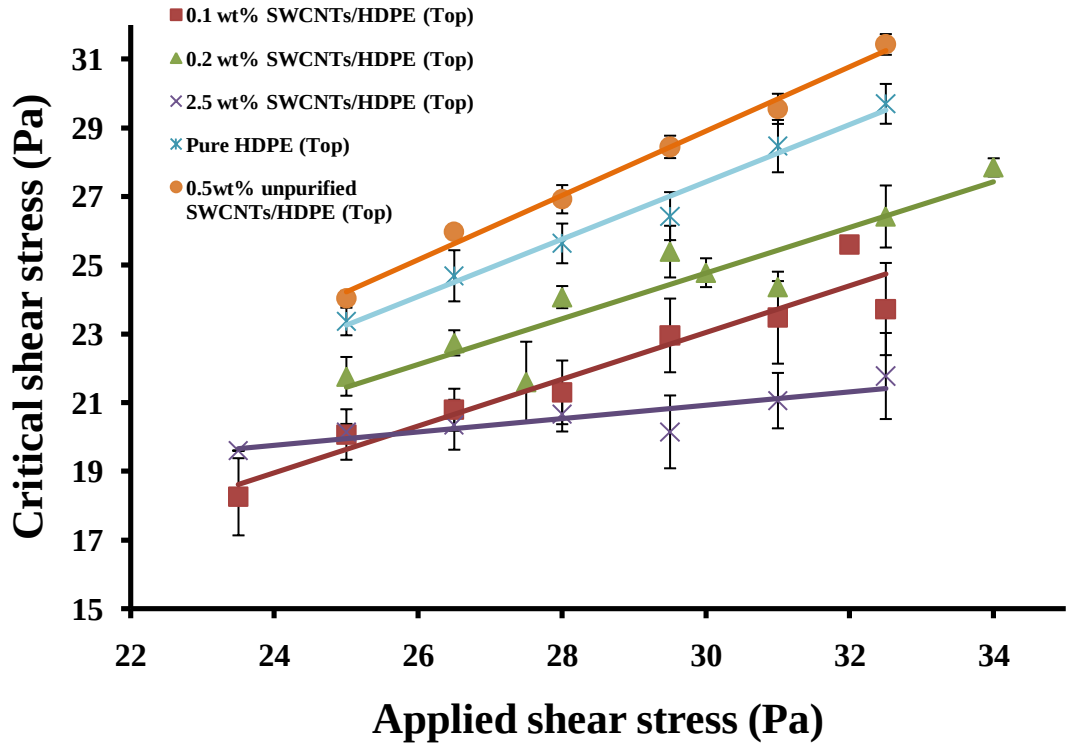

Fig. 23. Critical shear stress versus applied shear stress (top surface)

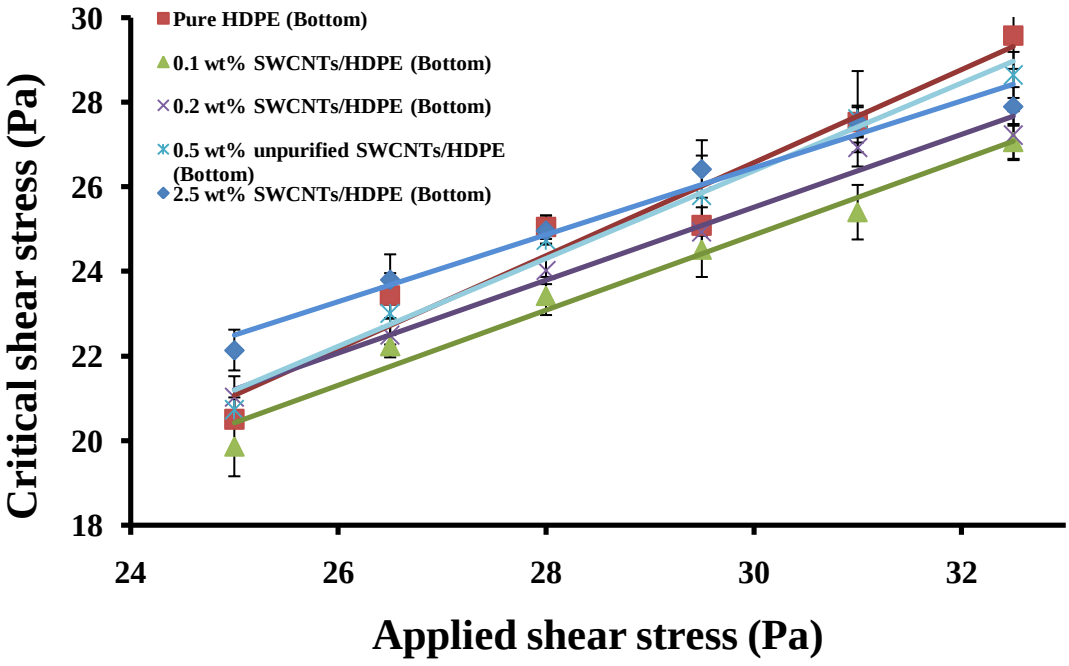

Fig. 24. Critical shear stress versus applied shear stress (bottom surface)

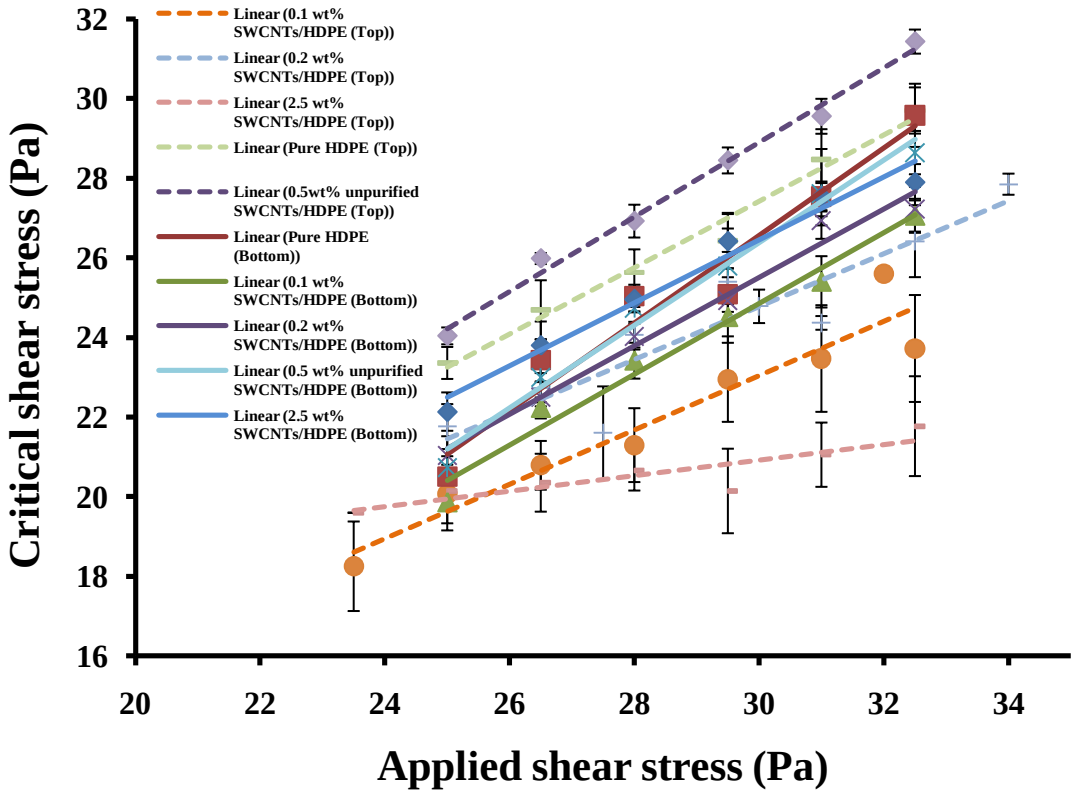

Fig. 25. Critical shear stress versus applied shear stress (top and bottom surfaces)

4.5. XRD test result

The chemical composition of every sample groups is similar. This had been proven by X-ray diffraction spectrum. Samples were set on a glass slide by using double sided tape. Since the sample film is thin, 40μm in thickness, the X-ray will penetrate the sample film as well the double sided tape. The XRD data for a composite specimen will include the noise of double sided tape. In order to eliminate this noise a glass slide with only double sided tape was scanned by XRD. The results show that the only crystallographic structure exists in the SWCNT-HDPE composites and HDPE samples are HDPE (Figs. 26 to 30). The chemical compositions of samples are nearly the same except the weight percent difference of SWCNTs. On the diffraction spectrum of a sample, including the noise, the highest peak was located at 60°. Based on the pure double-sided tape XRD diffraction scans, this peak belongs to the double sided tape (Fig. 31). The other two peaks, located near 21.6º and 24.1° are from HDPE [46-47]. These two peaks appear clearly in the spectrum when the noise was eliminated (Figs. 32 to 36).

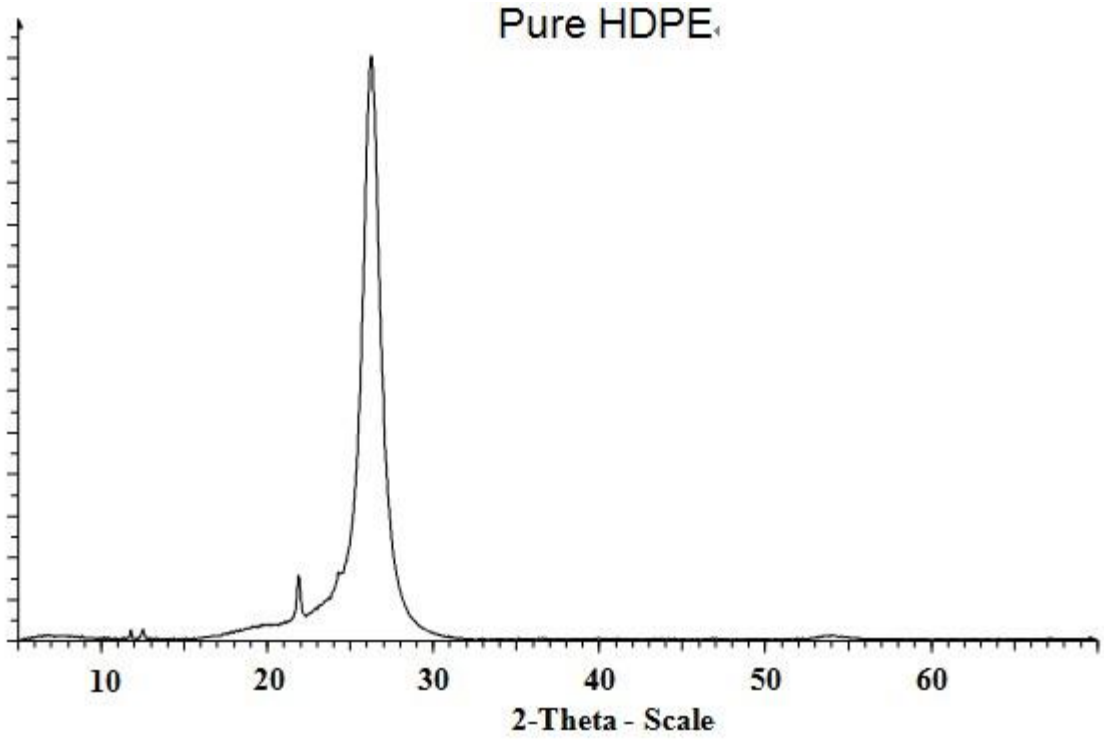

Fig. 26. XRD data for pure HDPE with noise

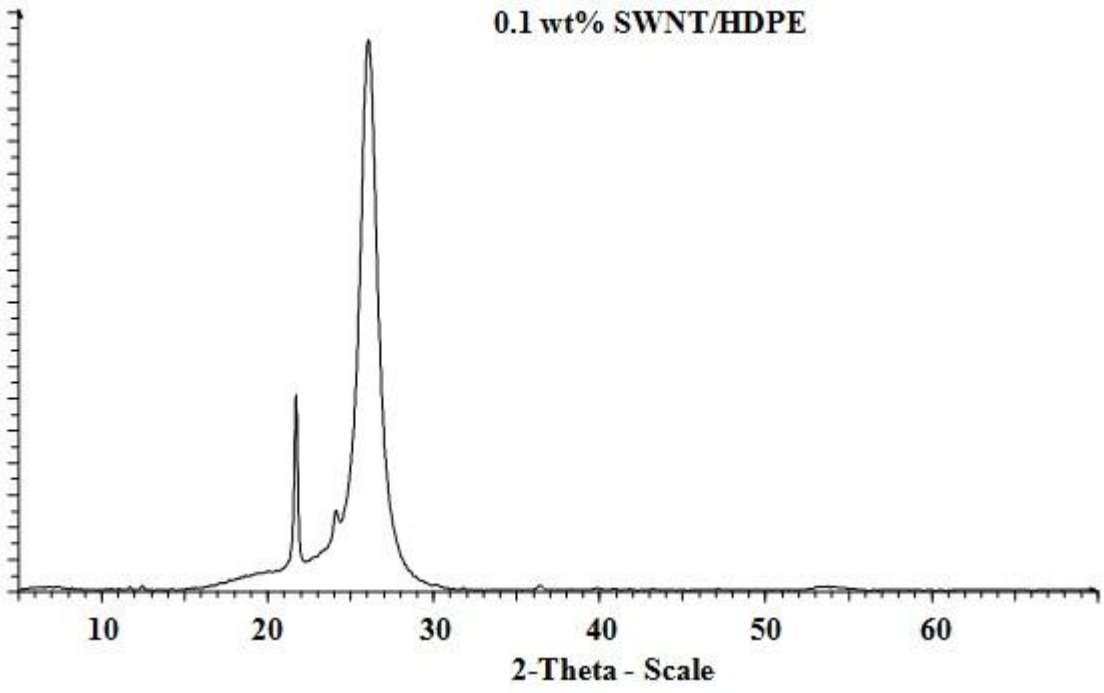

Fig. 27. XRD data for 0.1 %wt SWCNT-HDPE with noise

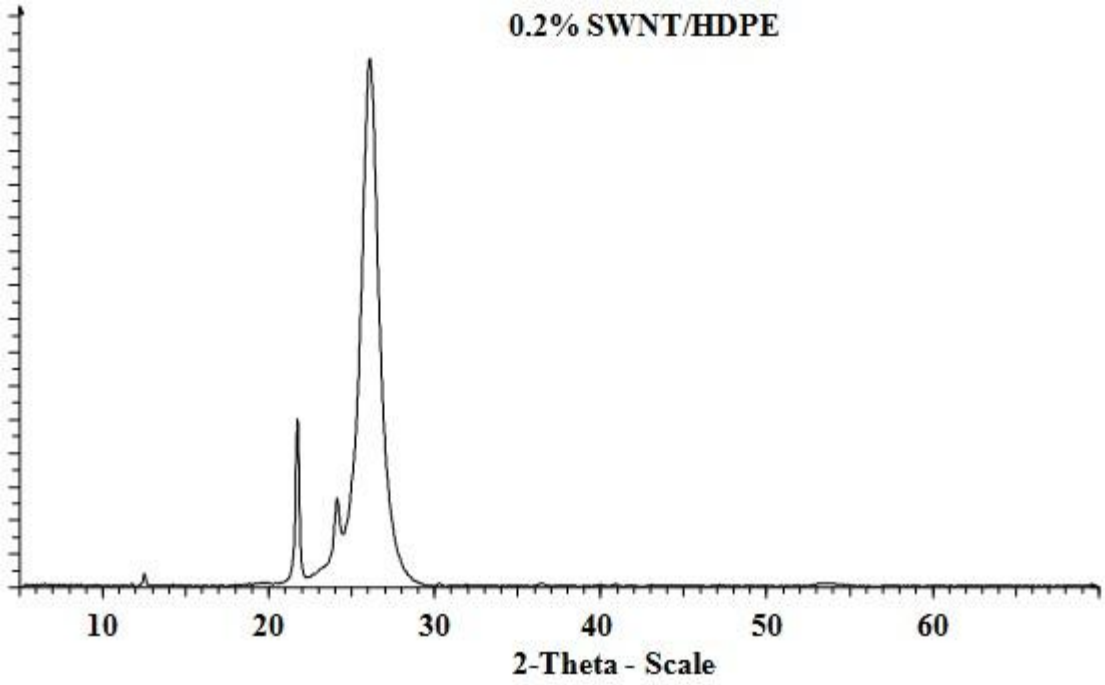

Fig. 28. XRD data for 0.2 %wt SWCNT-HDPE with noise

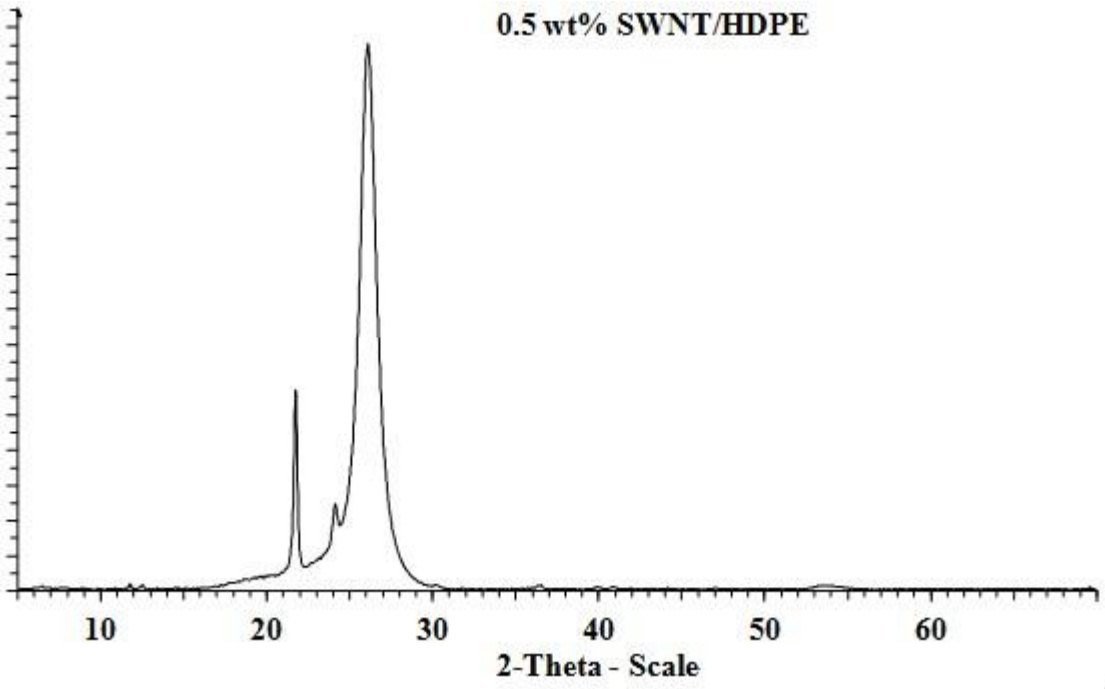

Fig. 29. XRD data for 0.5 %wt unpurified SWCNT-HDPE with noise

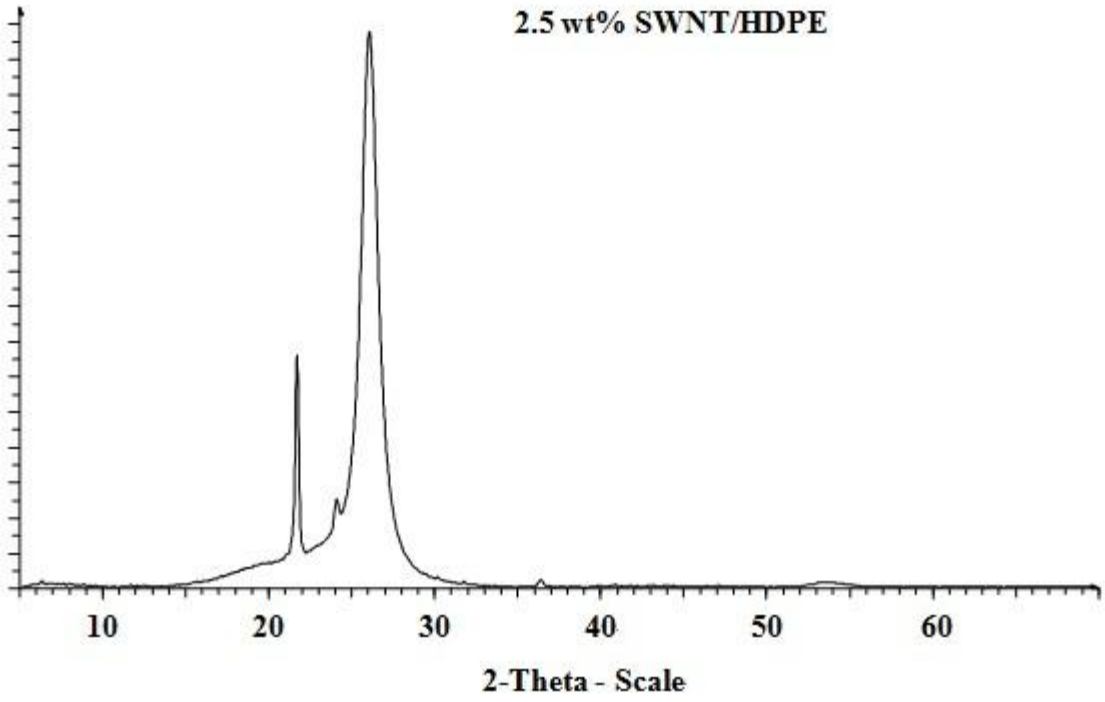

Fig. 30. XRD data for 2.5 %wt SWCNT-HDPE with noise

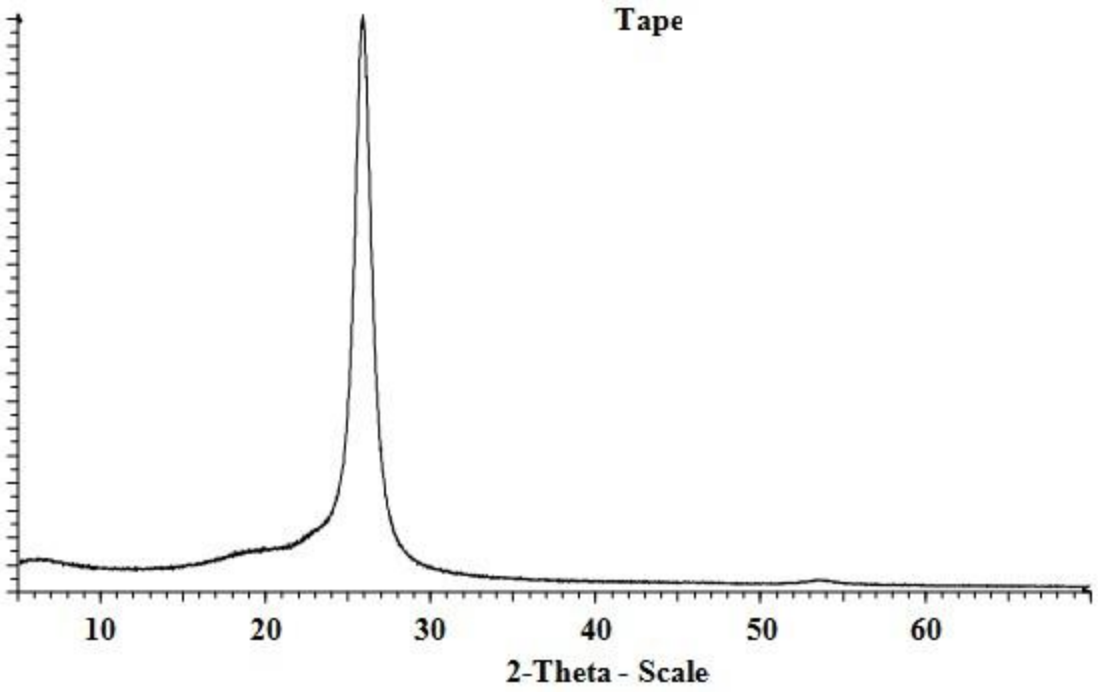

Fig. 31. XRD data for double sided tape

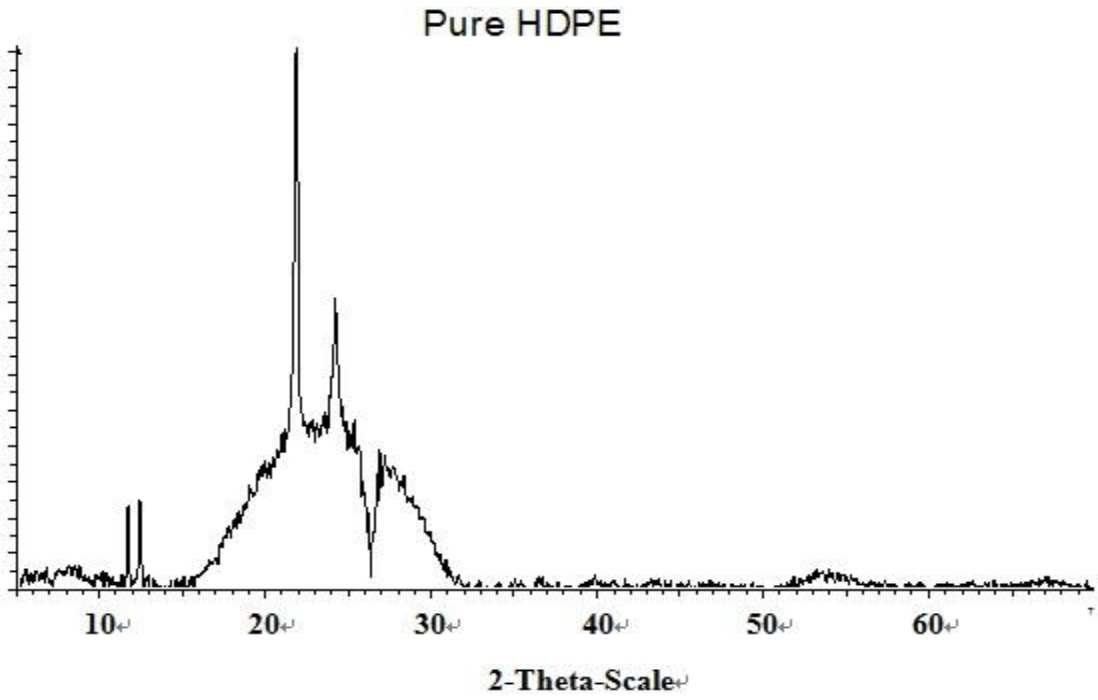

Fig. 32. XRD data for pure HDPE without noise

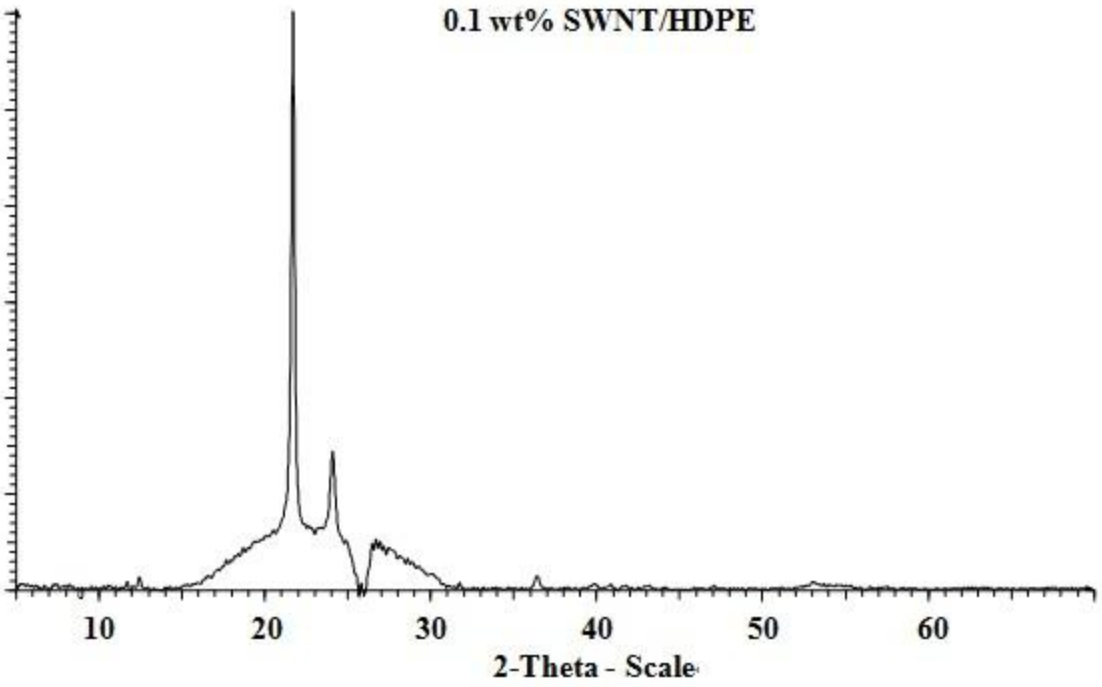

Fig. 33. XRD data for 0.1% wt SWCNT-HDPE without noise

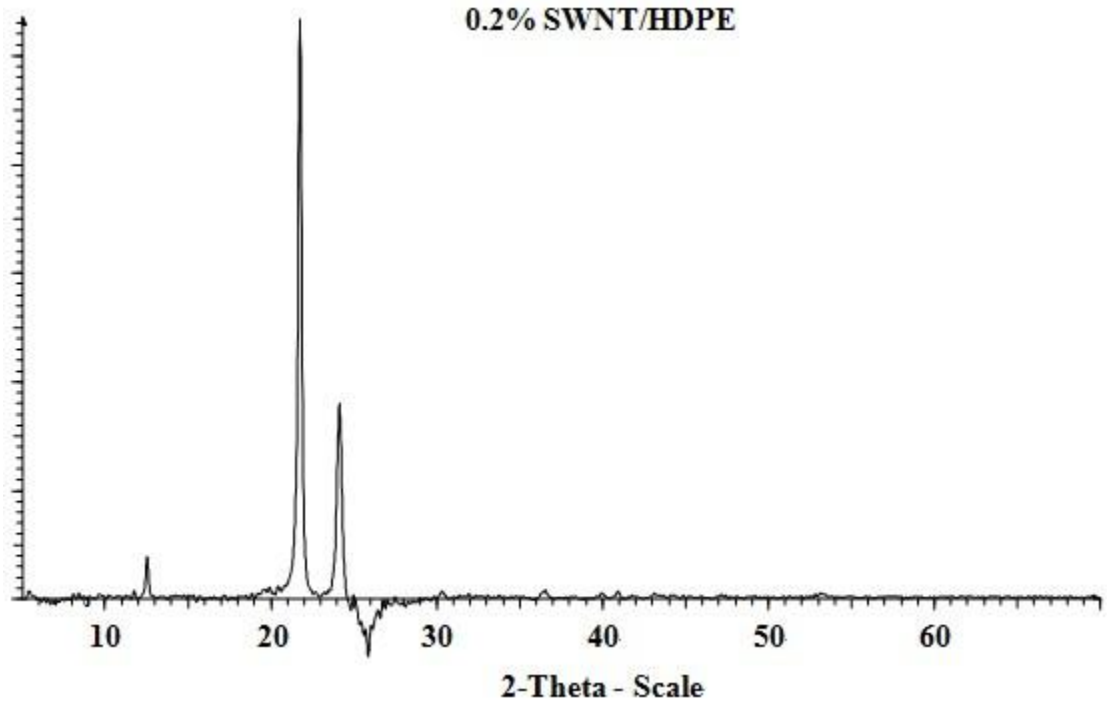

Fig. 34. XRD data for 0.2% wt SWCNT-HDPE without noise

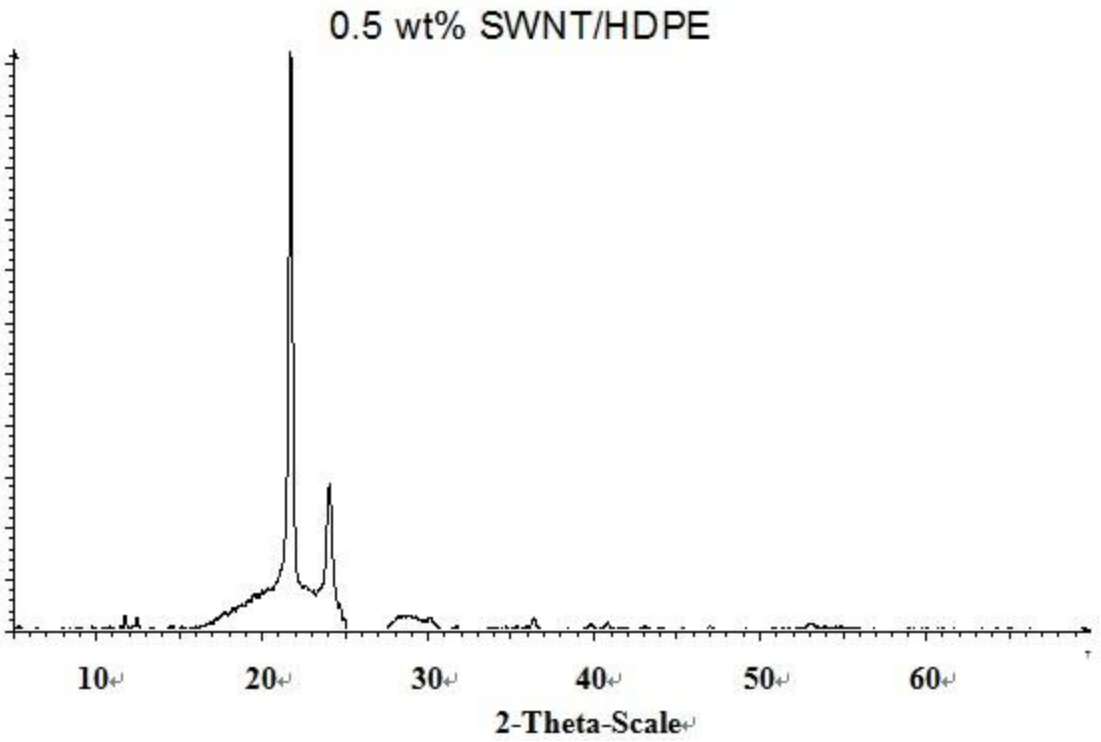

Fig. 35. XRD data for 0.5% wt unpurified SWCNT-HDPE without noise

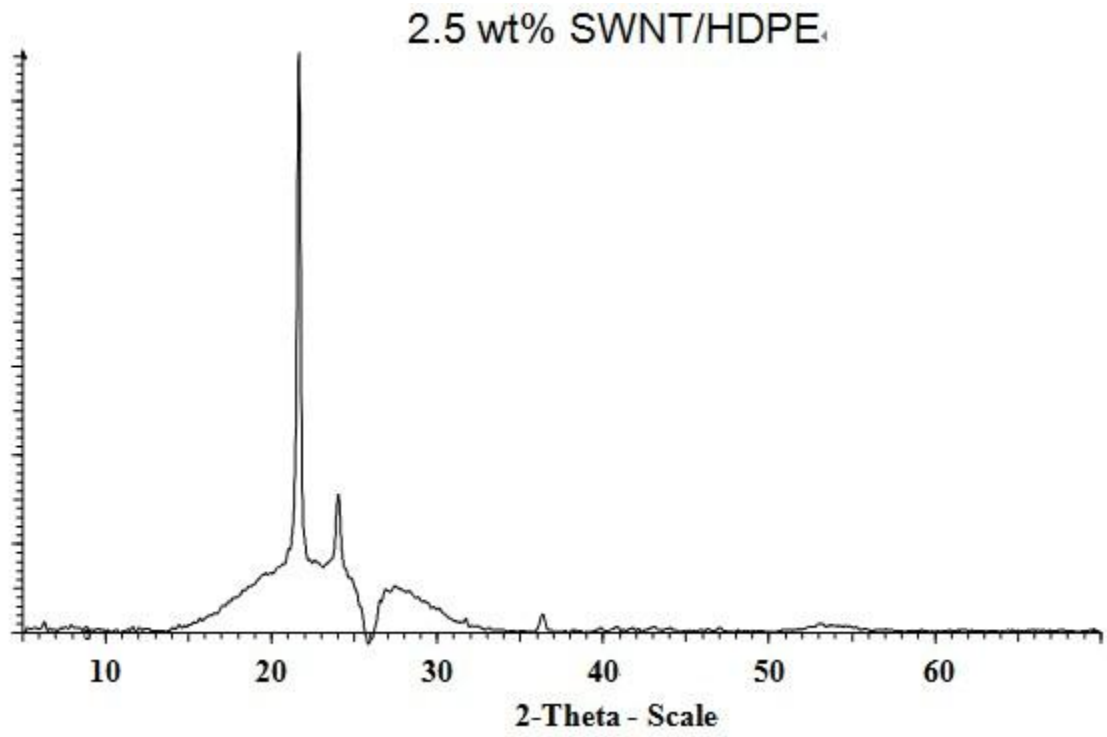

Fig. 36. XRD data for 0.5% wt SWCNT-HDPE without noise

4.6. AFM phase image

The AFM phase image for the top and bottom surfaces show different morphology and phase composition as shown in Fig. 37. The top surface shows only one phase while the bottom surface two phases. That is because the bottom surface was directly in contact with the glass plate during the fabrication process. The glass plate performed as preferential nucleation site for HDPE, which led to the heterogeneous nucleation.

Since the top surface was exposed to the air during their solidification process, the HDPE was naturally solidified without any influence. That is why their phase image shows only one phase, which represents homogeneous nucleation.

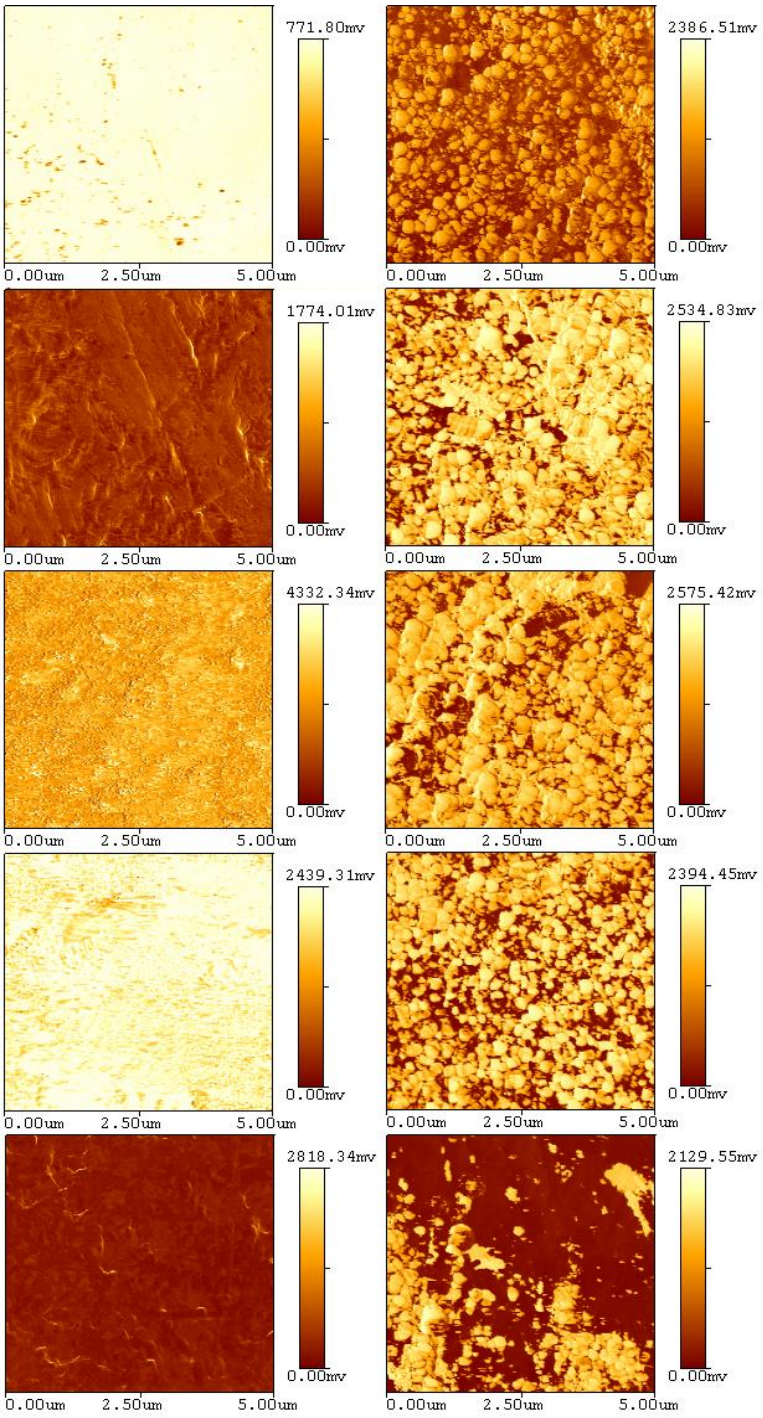

Fig. 37. Phase image for top (left) and bottom (right) surface
from top to bottom the samples are pure HDPE, 0.1 %, 0.2 %, 0.5 % unpurified and 2.5 %wt SWCNT-HDPE

CHAPTER V

ADHESION MECHANISMS

In this chapter, detailed discussions are provided based on experimental results in Chapter IV. The mechanisms of protein adhesion, effects of surface topography on the same will be analyzed.

5.1. SWCNT-HDPE composites

Potential effects of contact angle, surface conductivity, macroscopic and microscopic surface roughness are discussed here on protein adhesion.

5.1.1. Contact angle

Based on results in Fig. 21, contact angle do not show a specific trend with the adhesion force between the sample and the albumen. The bottom surface of every sample has a significantly higher contact angle than its top surface, i.e., more hydrophobic. If the contact angle were a dominant factor for protein adhesion, the top surface of every sample should have always had better adhesion with protein than the

bottom surface. However we found that there was no significant or consistent preference in protein adhesion for the top or bottom surface. The shear stress results (Fig. 25) showed that for some samples groups, such as pure HDPE and 0.5 %wt unpurified SWCNT-HDPE, their top surface had stronger adhesion with albumen than otherwise. For 0.1 %wt and 2.5 %wt sample groups, however, their bottom surface has better adhesion than their top surface. Moreover the adhesive strength of albumen to the rough and bottom surface of 0.2%wt samples is nearly the same. This indicated that the contact angle was not related to albumen adhesive strength on a surface.

5.1.2. Surface conductivity

Surface conductivity is not related to albumen adhesive strength on a surface. For the surface conductivity, the 0.5 %wt unpurified SWCNT-HDPE composite has much higher surface conductivity than other groups (Fig. 22). Although the top surface of 0.5 %wt unpurified SWCNT-HDPE composite shows stronger adhesive strength with albumen than all of the others, the bottom surface of 0.5 %wt composite does not show a significantly stronger adhesive strength with albumen than the other groups (Fig. 25).

5.1.3. Macro scale surface roughness

The adhesion between albumen and the sample surface is not related to macroscopic surface roughness. Because according to the macro scopic surface roughness test results the top surface of every sample has higher macro scale surface roughness than its bottom surface (Fig. 20). There is no consistent preference in protein adhesion for the top or bottom surface, which had already been discussed in Section 5.1.1. above. Overall the macroscopic surface roughness is not related to albumen adhesive strength.

5.1.4. Micro scale surface roughness

As seen in Fig. 38 micrometer length scale surface roughness have visible effects on adhesion for composite materials. In general, higher surface roughness in micro-scale improves the adhesion. This rule is applicable for nearly all of the sample groups independent of smooth or top surface testing. The exception is the top surface of 0.5 %wt unpurified SWCNT-HDPE and the top surface of pure HDPE. The adhesion is sensitive to the microscopic scale surface roughness (Fig. 38). The adhesive strength increases steadily with the micro-scale surface roughness tested by AFM. It is clear that the shear stresses are consistently high on the smooth surfaces.

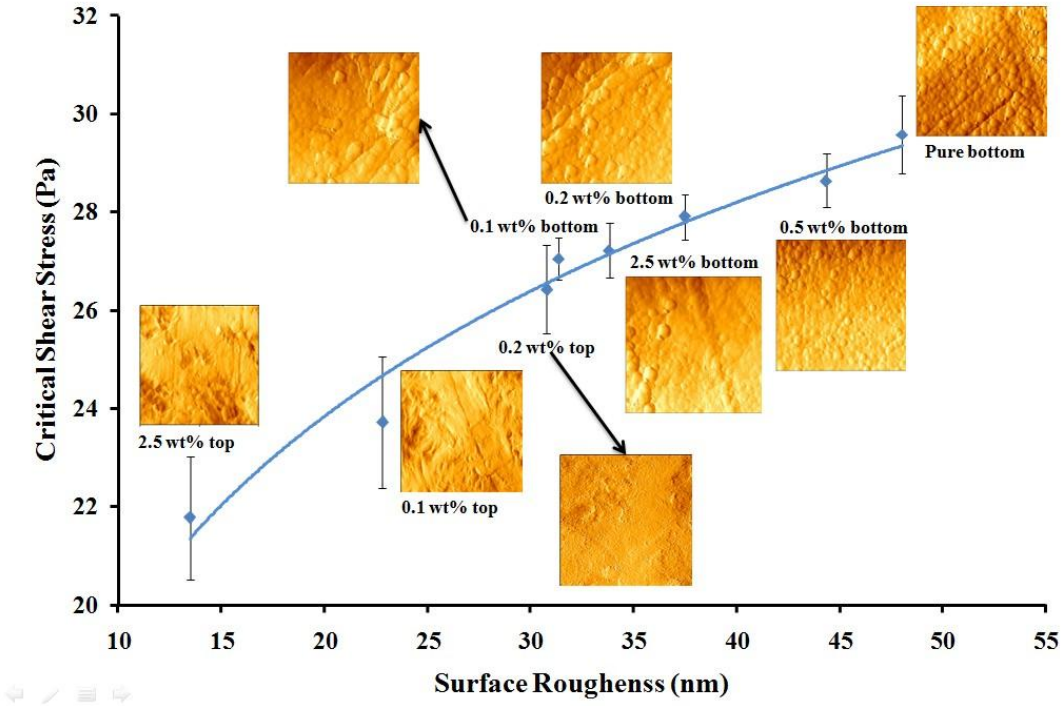

Fig. 38. Albumen sensitive to micro scale surface roughness (nm)

The critical shear stress in Fig. 26 was calculated from the test result of 32.5Pa applied shear stress. This value was selected because the fluid-film lubrication mechanism experienced at this applied shear stress, 32.5 Pa, is closest to that experienced by the artificial joint. In our test the shear rate reached the highest point of about 4500 s^{-1} when the applied shear stress by the spindle was 32.5 pa, which is closer to the shear rate experienced in hip implants under physiological walking conditions[48] than the other applied shear stress.

The Fig. 39 helps to explain how the increase in micro-scale surface roughness increases protein adhesion. Protein molecule (2-5Å) [40] is much smaller than those

micro-scale surface features (100-500nm). It can only sense the micro-scale surface roughness instead of macro-scale surface roughness. For the protein molecule, the macro-scale surface roughness can be considered as surface waviness. The protein coating was removed layer by layer via the rotating water flow. A rough surface has larger peak-to-valley distance. The protein accumulated in the valley will be hard to remove. This is because when the water flows across the surface, the peak prevents the water from flowing into the valley hence to remove the protein. The surface waviness, however, cannot influence the water flow as the surface roughness. That is why the sample with higher micro-scale surface roughness has stronger adhesion with the albumen coating.

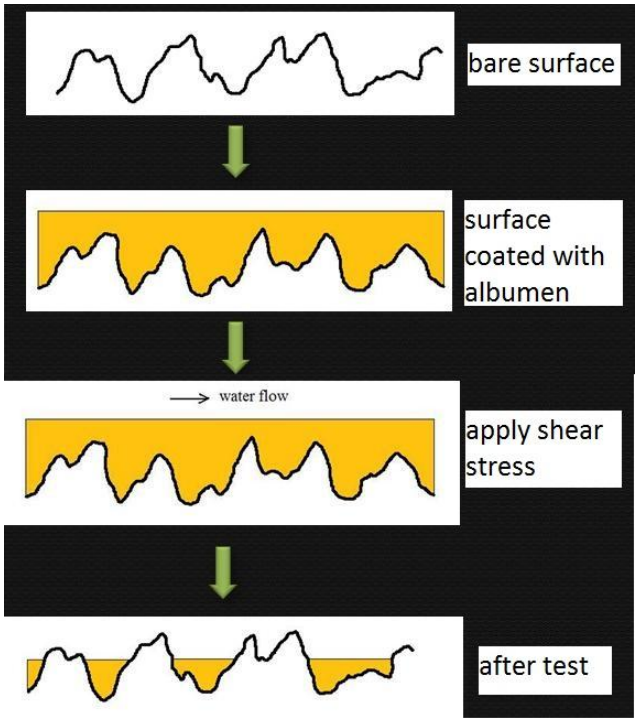

Fig. 39. Remove process of albumen coating

During the SWCNT-HDPE sample fabrication process, samples were allowed to cure over a ceramic glass plate. This process gave the bottom surface of all samples similar surface topography and surface roughness. The AFM scans of the bottom surface of all samples are showed (in Fig. 38). Samples have similar surface topography where the micro-scale showed significant bumps. The formation of this surface topography is because the bottom surface directly contacted the heat-resistant ceramic glass plate during the solution casting process. The surface topography on the ceramic glass plate printed onto the bottom surface. Since size of albumen is relevant to the fine scale roughness. The similar roughness resulted in the similar adhesive strength as observed in Fig. 24. On the contrary, for the top surfaces, the dominating factors for the formation of the surface depend largely on the SWCNTs concentration and purity. This was proven by Fig. 23. That is why there is a minor difference in the critical shear stress of the samples tested on their bottom surface. But there is a significant and clear difference on the critical shear stress of the samples tested on their top surface (shown in Fig. 25).

5.1.5. Spherulitic crystallinity

The crystalline morphology for pure HDPE is the well-known spherulitic morphology[49]. On the top surface of pure HDPE this feature was observed by AFM scan and optical profilometer scan. Fig. 40 shows the obvious spherulitic morphology of

the pure HDPE on its top surface shown at 25µm x 25µm scale and 0.14mm x 0.11mm scale. These features were about 10 µm in diameter. The SWCNTs, however, can act as the nucleation site of HDPE and impinge the fully formation of spherulitic crystals. Instead the HDPE crystallizes around SWCNTs. This influence makes spherulitic crystallinity structure lose that bump feature and become relatively more flat. That is why the spherulitic bump structure cannot be clearly observed on the top surface for any of the SWCNT-HDPE composite samples.

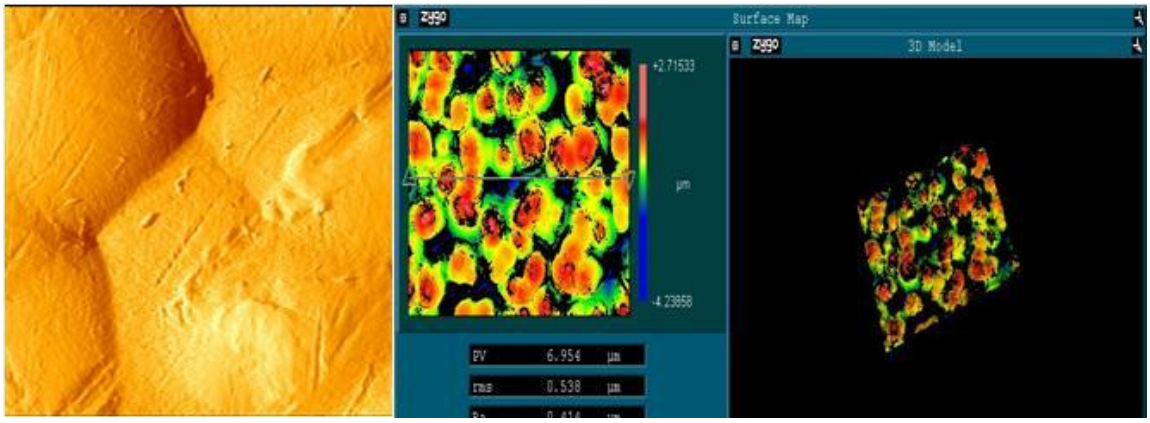

Fig. 40. Spherulitic feature on the top surface of pure HDPE sample: AFM 25µm x 25µm (left) and optical profilometer 0.14mm x 0.11mm (right)

Spherulitic crystallinity also exists on the bottom surface of every sample. The edge of that crystal structure, however, is covered by small bumps that originated from the glass plate. This coverage make spherulitic crystallinity bump feature cannot be clearly observed by AFM or optical profilometer on the bottom surface. Although the spherulitic crystalline structure bump feature is not clearly shown on the bottom surface

of pure HDPE, they still influence the macro scale surface roughness test results. The results from the optical profilometer indicate that the bottom surface of pure HDPE has higher macro-scale surface roughness than the bottom surface of other composites (Fig. 20).

The influence of spherulitic crystallinity structure on surface roughness is not only limited to macro scale. Fig. 38 shows that pure HDPE has higher micro scale surface roughness that other composites on the bottom surface. In summary, spherulitic crystallinity gives pure HDPE a higher macroscopic and microscopic surface roughness than composite samples for both smooth and top surface.

5.1.6. Nano-porous surface structures

The previous section discussed about the effects of surface roughness and topography on albumen adhesion. It concluded that higher micro-scale surface roughness improves the adhesion. The question arose on why the top surface of 0.5 %wt unpurified SWCNTs-HDPE samples had the strongest adhesion followed by the top surface of pure HDPE?

The AFM scan in Fig. 41 shows that the top surface of the 0.5 %wt unpurified SWCNTs-HDPE composite and the pure HDPE samples have a special porous structure. The pores on the surface are in the nano-scale (100-150nm) and will be referenced from now on as nano-porous structure. This nano-porous structure promoted the strongest

adhesion of albumen, as shown in Fig. 25. On the top surface of 0.5 %wt unpurified SWCNTs-HDPE composite, there are high dense pores.

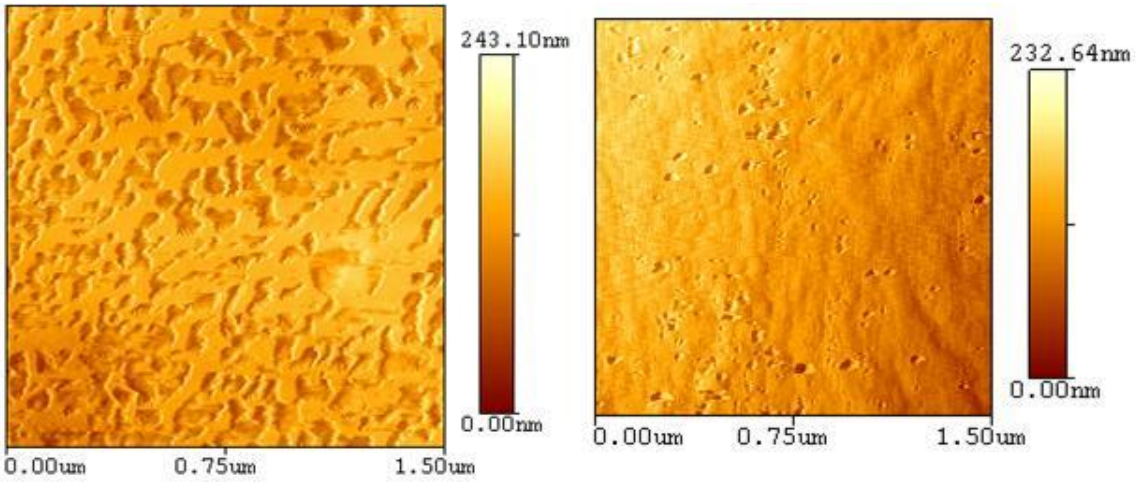

Fig. 41. AFM scan for the top surface of 0.5 unpurified SWCNTs/ HDPE composite (up) and pure HDPE (down) sample (1.5μm x 1.5μm)

This nano-porous structure can also be observed on the top surface of pure HDPE but its density is much less than 0.5 %wt unpurified samples. The porosity ratio, calculated from equation (4), is used to quantify this structure:

$$\emptyset = \frac{A_V}{A_T} \qquad (4)$$

where Φ is the porosity ratio, A_V is total project area of pores and A_T is the total surface area of the sample surface. The porosity ratio for unpurified SWCNT-HDPE and pure HDPE are 31.4 % and 3.1 % respectively. The nano-porous structure is beneficial for the enhancement of adhesion between sample and albumen. The small pores work as the

protection sites for albumen molecules. Nano-pores are surrounded by a “mesa” (elevated flat top). These mesas act as a wall to protect the albumen collected in the nano-pores.

The high density nano-porous structure formed on the top surface of unpurified SWCNT-HDPE composites is caused by the unpurified SWCNTs. The purification process for the SWCNTs in this research is nitric acid reflux and gas phase oxidization. These two processes, especially the nitric acid reflux process, underwent for 16 hours. This was expected to change the entangled agglomeration structure of the unpurified SWCNTs and to extend their alignment[50]. These alignments cannot make the top surface of SWCNT-HDPE composites have nano-porous structure (Fig. 38). Comparatively the entangled structure of unpurified SWCNTs led to the nano-porous structure on unpurified 0.5 %wt SWCNT-HDPE composites (Fig. 41).

5.1.7. Top and bottom surface comparison

Figs. 42 to 46 are the line profiles for the comparison of each sample on its top and bottom surfaces. For the top surface of the pure HDPE sample, there existed small amount nano-porous structures that apparently were sufficient to improve the adhesion (Fig. 42). A high density nano-porous structure was found on the top surface of the 0.5 %wt SWCNTs-HDPE composite (shown in Fig. 45) which promotes adhesion. For the other three groups as shown in Figs. 43, 44, and 46, we did not find any nano-porous structure. In such the micro scale surface roughness dominates. As discussed earlier, the surface roughness was affected by two factors, the SWCNTs-induced crystallization of HDPE and the glass ceramic substrate. For the 0.2 %wt sample, the bottom surface featured many small bumps while the top surface nano scale peaks. Since their micro scale surface roughness had similar adhesion, their adhesive strength with protein is similar. On the top surface of 2.5 %wt SWCNT-HDPE composites, SWCNTs severely impinge the formation of spherulitic crystallinity. This is associated with the concentration of SWCNTs resulting in very low micro scale surface roughness.

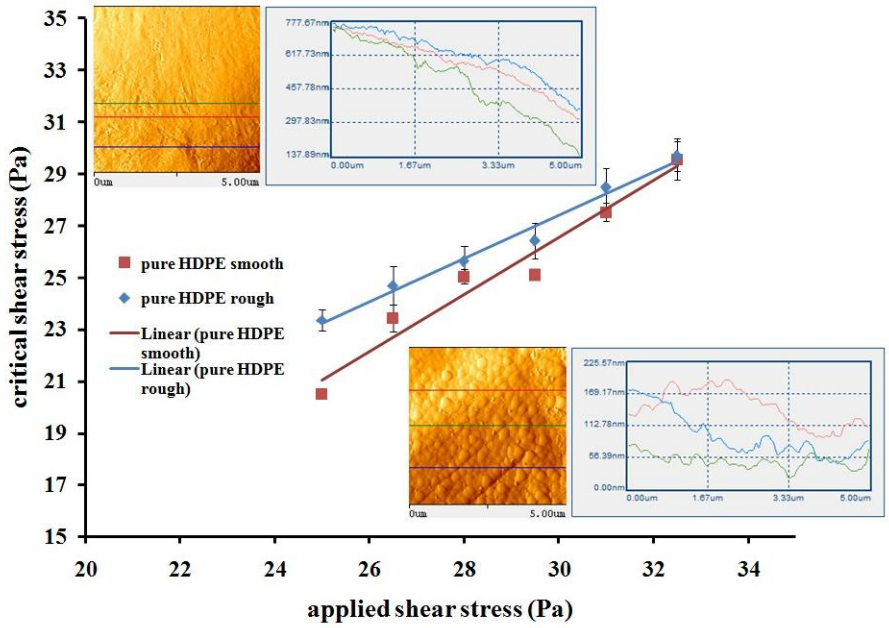

Fig. 42. Comparison of pure HDPE in 5µm x 5 µm for its top (up) and bottom surface (down)

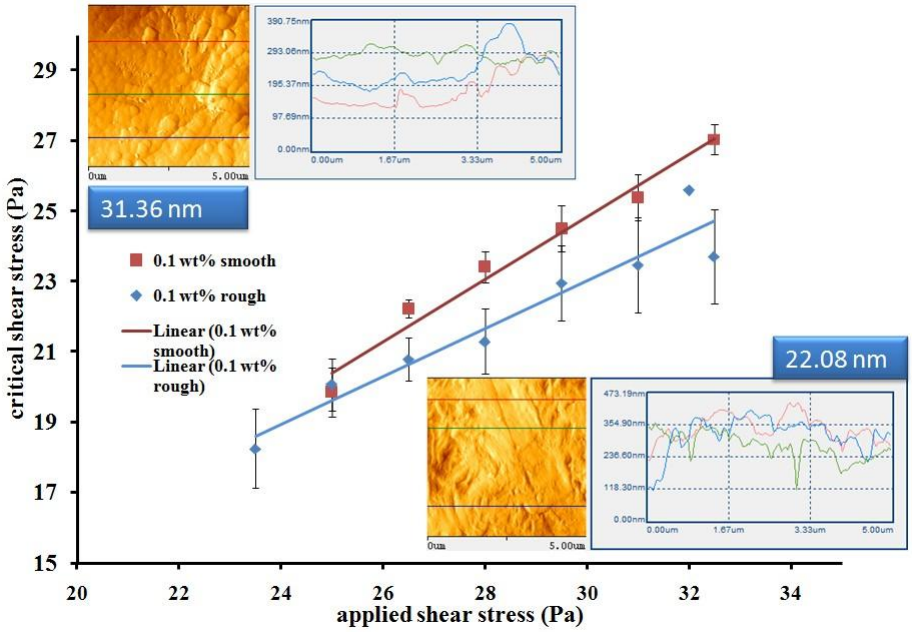

Fig. 43. Comparison of 0.1 %wt SWCNTs/HDPE in 5µm x 5 µm for its top (down) and bottom surface (up)

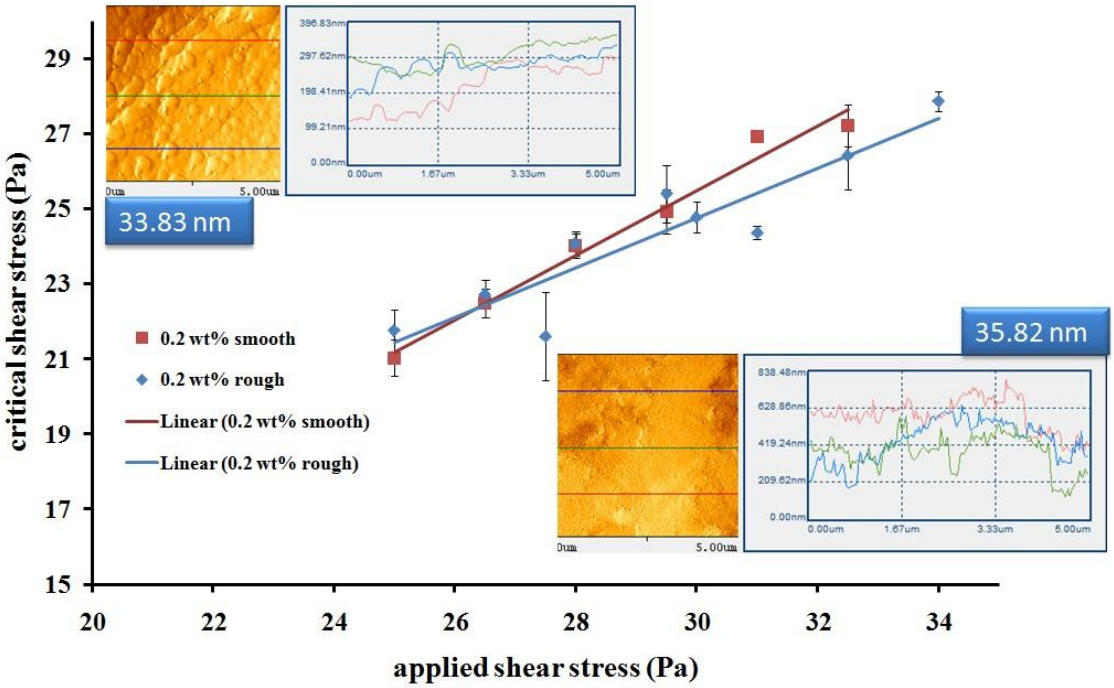

Fig. 44. Comparison of 0.2 %wt SWCNTs/HDPE in 5µm x 5 µm for its top (down) and bottom surface (up)

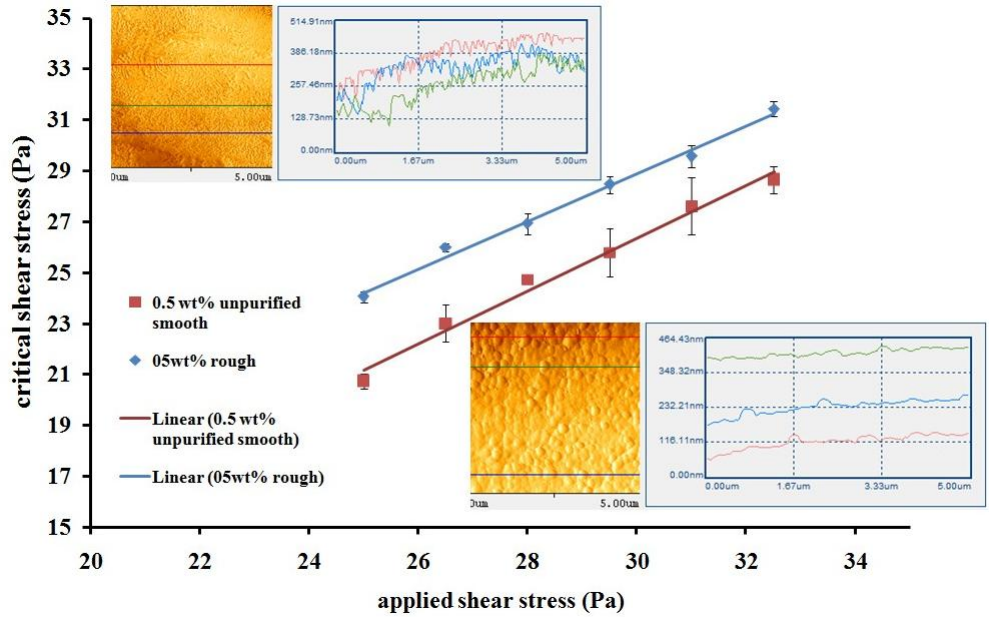

Fig. 45. Comparison of 0.5 %wt unpurified SWCNTs/HDPE in 5µm x 5 µm for its top (up) and bottom surface (down)

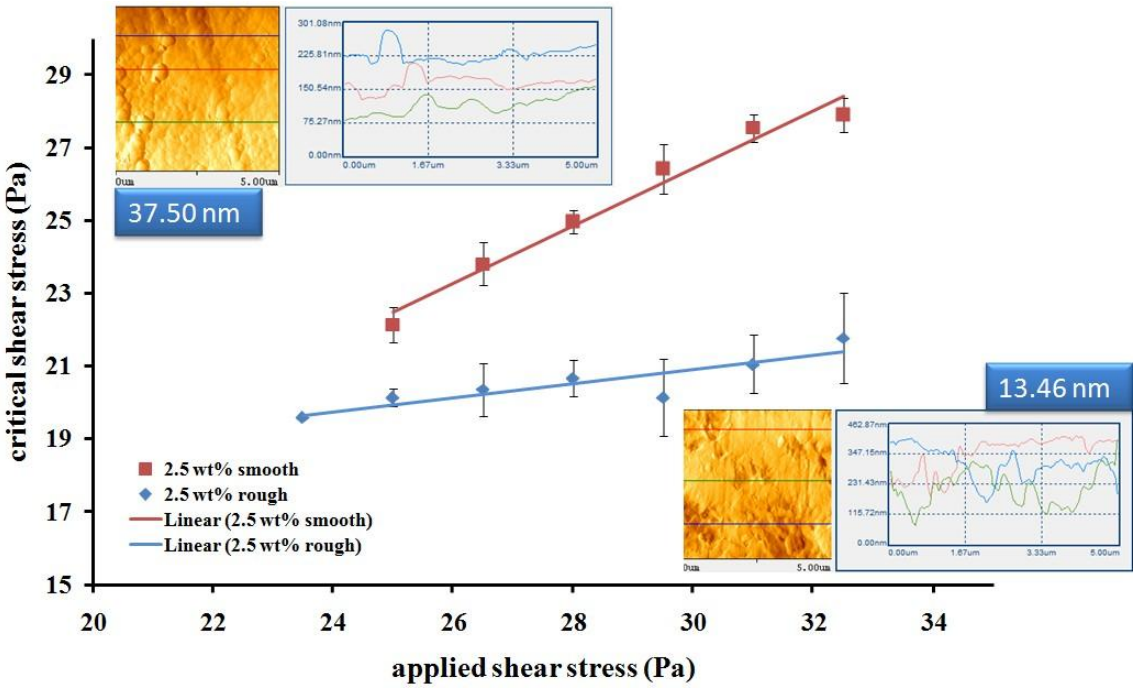

Fig. 46. Comparison of 2.5 %wt SWCNTs/HDPE in 5μm x 5 μm for its top (down) and bottom surface (up)

5.2. Ti-C:H and Ti6Al4V

The comparison between Ti-C:H coating and Ti6Al4V (Fig. 47) shows that the nano-porous structure found on Ti-C:H coating promote adhesion. This proves the effectiveness of nano-porous toward protein adhesion. As seen in Fig. 47, the Ti6Al4V had even stronger adhesion than we expect. That is because it has been shown in Fig. 21 that the surface of Ti6Al4V is more hydrophilic than Ti-C:H. It has been found that hydrophilic surfaces preferentially adsorb protein than do hydrophobic surfaces [4]. Our result is in correlation with the report.

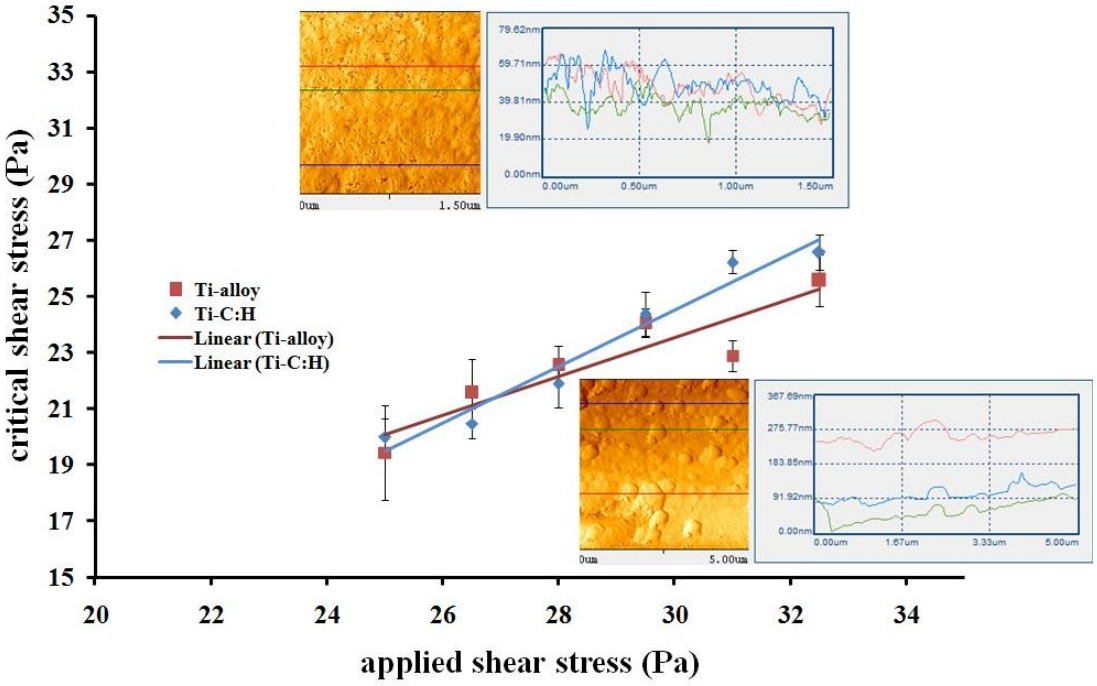

Fig. 47. Comparison of Ti6Al4V (down) in 5µm x 5 µm
and Ti-C:H (up) in 1.5µm x 1.5 µm

CHAPTER VI

CONCLUSIONS AND FUTURE RECOMMENDATION

6.1. Conclusions

This research utilized a rheological methodology to quantify the adhesive strength of albumen to 0.1 %, 0.2 %, 0.5 % unpurified and 2.5 %wt SWCNTs enhanced HDPE, pure HDPE, Ti-C:H coating, and Ti alloy sample surfaces. Experimental investigation was carried out using fluid shear measurement. Effects of morphological and physical properties of those materials on protein adhesion were studied.

It was found that the 0.5 %wt unpurified SWCNTs–HDPE composite has stronger adhesion with albumen than pure HDPE. The Ti-C:H coating has stronger adhesion with albumen than Ti-alloy.

Experimental results showed that the porous structure, formed on the top surface of 0.5 %wt unpurified SWCNTs enhanced HDPE, promoted adhesion of protein. It was due to the trapping of those molecules inside the pores. Similar surface topography was also found on the HDPE and Ti-C:H coated surfaces.

The present research indicated that nano-porous surface structure could store synovial fluid and benefit the lubrication of artificial joints. The present research is beneficial to design the surface topography in micro and/or nano-meter length scale. With improved adhesion and better lubricated implants, the service life and performance of artificial joints are expected to be significantly improved.

6.2. Future recommendation

The methodology used in the present research can be applied to different kinds of materials. This method can quantify the adhesive force of cells or proteins to any sample surface and effectively compare them. It was found that surface conductivity, macro scale surface roughness, and contact angle do not directly influence the adhesion strength of albumen to the surface. Other neglectable structures and surface properties should be further identified. In addition, theoretical analysis should be carried out in order to be able to predict the surface and its effects on adhesion of various biological entities.

REFERENCES

[1] Kurtz SM, Stein HL, Redeker G. Meeting the joint replacement challenge with UHMWPE. Medical Device and Diagnostic Industry. 2005;27:110-7.

[2] Sott AH, Rosson JW. The influence of biomaterial on patterns of failure after cemented total hip replacement. International Orthopaedics. 2002;26(5):287-90.

[3] Maurer TB, Ochsner PE, Schwarzer G, Schumacher M. Increased loosening of cemented straight stem prostheses made from titanium alloys. An analysis and comparison with prostheses made of cobalt-chromium-nickel alloy. International Orthopaedics. 2001;25(2):77-80.

[4] Heuberger MP, Widmer MR, Zobeley E, Glockshuber R, Spencer ND. Protein-mediated boundary lubrication in arthroplasty. Biomaterials. 2004;26(10):1165-73.

[5] Su SH, Hua ZK, Zhang JH. Design and mechanics simulation of bionic lubrication system of artificial joints. Journal of Bionic Engineering. 2006;3(3):155-60.

[6] Hoseini A, Jedenmalm A, Boldizar A. Tribological investigation of coatings for artificial joints. Wear. 2008;264(11-12):958-66.

[7] Ramakrishna S, Mayer J, Wintermantel E, Leong KW. Biomedical applications of polymer-composite materials: a review. Composites Science and Technology. 2001;61(9):1189-224.

[8] Andrews R, Weisenberger MC. Carbon nanotube polymer composites. Current Opinion in Solid State and Materials Science. 2004;8(1):31-7.

[9] Wang MW, Hsu TC, Zheng JR. Sintering orocess and mechanical property of MWCNTs/HDPE bulk composite. Polymer-Plastics Technology and Engineering. 2009;48(8):821-6.

[10] Ahir SA, Huang YY, Terentjev EM. Polymers with aligned carbon nanotubes: Active composite materials Polymer. 2008;49(18):3841-54.

[11] Spitalsky Z, Tasis D, Papagelis D, Galiotis C. Carbon nanotube–polymer composites: Chemistry, processing, mechanical and electrical properties.

Progress in Polymer Science. 2010;35(3):357-401.

[12] Johnson BB, Santare MH, Novotny JE, Advani SG. Wear behavior of carbon nanotube/high density polyethylene composites. Mechanics of Materials. 2009;41(10):1108-15.

[13] Pye AD, Lockhart DEA, Dawson MP, Murray CA, Smith AJ. A review of dental implants and infection. Journal of Hospital Infection. 2009;72(2):104-10.

[14] Weber HP, Cochran DL. The soft tissue response to osseointegrated dental implants. The Journal of Prosthetic Dentistry. 1998;79(1):79-89.

[15] Guéhennec LL, Soueidan, Layrolle P, Amouriq Y. Surface treatments of titanium dental implants for rapid osseointegration. Dental Materials. 2007;23(7):844-54.

[16] Myshin HL, Wiens JP. Factors affecting soft tissue around dental implants: A review of the literature. The Journal of Prosthetic Dentistry. 2005;94(5):440-4.

[17] Bieniaś J, Surowska B, Stoch A, Matraszek H, Walczak M. The influence of SiO2 and SiO2–TiO2 intermediate coatings on bond strength of titanium and Ti6Al4V alloy to dental porcelain Dental Materials. 2009;25(9):1128-35.

[18] Polcar T, Vitu T, Cvrcek L, Novak R, Vyskocil J, Cavaleiro A. Tribological behaviour of nanostructured Ti-C:H coatings for biomedical applications. Solid State Sciences. 2009;11(10):1757-61

[19] Vitu T, Polcar T, Cvrcek L, Novak R, Macak J, Vyskocil J, Cavaleiro A. Structure and tribology of biocompatible Ti–C:H coatings Surface and Coatings Technology. 2008;202(22-23):5790-3.

[20] Feng B, Cao DM, Meng WJ, Xu J, Tittsworth RC, Rehn LE, Baldo PM, Doll GL. Characterization of microstructure and mechanical behavior of sputter deposited Ti-containing amorphous carbon coatings Surface and Coatings Technology. 2001;148(2-3):153-62.

[21] Meng WJ, Tittsworth RC, Rehn LE. Mechanical properties and microstructure of TiC/amorphous hydrocarbon nanocomposite coatings. Thin Solid Films. 2000;377-378(1):222-32.

[22] Mongkolwongrojn M, Wongseedakaew K, Kennedy FE. Transient elastohydrodynamic lubrication in artificial knee joint with non-Newtonian fluids Tribology International. 2009;43(5-6):1017-26.

[23] Jhurani SM, Higgs CF. An elastohydrodynamic lubrication (EHL) model of wear particle migration in an artificial hip joint. Tribology International. 2009:1326-38.

[24] Kidoaki S, Matsuda T. Adhesion forces of the blood plasma proteins on self-assembled monolayer surfaces of alkanethiolates with different functional groups measured by an atomic force microscope. American Chemical Society. 1999;15(22):7639-46.

[25] Roba M, Naka M, Gautier E, Spencer ND, Crockett R. The adsorption and lubrication behavior of synovial fluid proteins and glycoproteins on the bearing-surface materials of hip replacements Biomaterials. 2009;30(11):2072-8.

[26] Serro AP, Degiampietro K, Colaço R, Saramago B. Adsorption of albumin and sodium hyaluronate on UHMWPE: A QCM-D and AFM study. Colloids and Surfaces B: Biointerfaces. 2010;78(1):1-7.

[27] Huang Y, Lü X, Jingwu M, Huang N. In vitro investigation of protein adsorption and platelet adhesion on inorganic biomaterial surfaces. Applied Surface Science. 2008;255(2):257-9.

[28] Galli C, Coen MC, Hauert R, Katanaev VL, Gröning P, Schlapbach L. Creation of nanostructures to study the topographical dependency of protein adsorption Colloids and Surfaces B: Biointerfaces. 2002;26(3):256-67.

[29] Deligianni DD, Katsala N, Ladas S, Sotiropoulou D, Amedee J, Missirlis YF. Effect of surface roughness of the titanium alloy Ti–6Al–4V on human bone marrow cell response and on protein adsorption Biomaterials. 2001;22(11):1241-51.

[30] Rocha A, Hahn M, Liang H. Critical fluid shear stress analysis for cell–polymer adhesion. Journal of Materials Science. 2009;45(3):811-7.

[31] Fritsche A, Luethen F, Lembke U, Finke B, Zietz C, Rychly J, Mittelmeier W, Bader R. Measuring bone cell adhesion on implant surfaces using a spinning disc device. Materialwissenschaft und Werkstofftechnik. 2010;41(2):83-8.

[32] Ando J, Nomura H, Kamiya A. The effect of fluid shear stress on the migration and proliferation of cultured endothelial cells Microvascular Research. 1987;33(1):62-70.

[33] Cai K, Bossert J, Jandt KD. Does the nanometre scale topography of titanium influence protein adsorption and cell proliferation? Colloids and Surfaces B:

Biointerfaces. 2006;49(2):136-44.

[34] Denis FA, Hanarp P, Sutherland DS, Gold J, Mustin C, Rouxhet PG, Dufrêne YF. Dufrêne. Protein Adsorption on Model Surfaces with Controlled Nanotopography and Chemistry. American Chemical Society. 2002;18(3):819-28.

[35] Wong M, Eulenberger J, Schenk R, Hunziker E. Effect of surface topology on the osseointegration of implant materials in trabecular bone. Journal of Biomedical Materials Research. 1995;29(12):1567-75.

[36] Buser D, Schenk RK, Steinemann S, Fiorellini JP, Fox CH, Stich H. Influence of surface characteristics on bone integration of titanium implants. A histomorphometric study in miniature pigs. Journal of Biomedical Materials Research. 1991;25(7):889-902.

[37] Deligianni DD, Katsala ND, Koutsoukos PG, Missirlis YF. Effect of surface roughness of hydroxyapatite on human bone marrow cell adhesion, proliferation, differentiation and detachment strength. Biomaterials. 2001;22(1):87-96.

[38] Bronikowski MJ, Willis PA, Colbert DT, Smith KA, Smalley RE. Gas-phase production of carbon single-walled nanotubes from carbon monoxide via the HiPco process: A parametric study. American Vacuum Society. 2001;19(4):1800-5.

[39] Chiang IW, Brinson BE, Huang AY, Willis PA, Bronikowski MJ, Margrave JL, Smalley RE, Hauge RH. Purification and characterization of single-wall carbon nanotubes (SWNTs) obtained from the gas-phase decomposition of CO (HiPco Process). American Chemical Society. 2001;105(35):8297-301.

[40] Mine Y. Recent advances in the understanding of egg white protein functionality. Trends in Food Science & Technology. 1995;6(7):225-32.

[41] Weijers M, Velde F, Stijnman A, Pijpekamp A, Visschers RW. Structure and rheological properties of acid-induced egg white protein gels. Food Hydrocolloids. 2006;20(2-3):146-59.

[42] Shipman RWG, Denn MM, Keunings R. Free-surface effects in torsional parallel-plate rheometry. American Chemical Society. 1991;30(5):918-22.

[43] Schlichting H, Gersten K. Genzschicht-Theorie. Springer-Verlag Berlin Heidelberg. 1997.

[44] Garg VK, Szeri AZ. Fluid flow and heat transfer between finite rotating disks. International Journal of Heat and Fluid Flow. 1993;14(2):155-63.

[45] Leshev I, Peev G. Film flow on a horizontal rotating disk Chemical Engineering and Processing. 2003;42(11):925-9.

[46] Sui G, Zhong WH, Ren X, Wang XQ, Yang XP. Structure, mechanical properties and friction behavior of UHMWPE/HDPE/carbon nanofibers. Materials Chemistry and Physics. 2009;115(1):404-12.

[47] Qiao M, Ran Q, Wu S, Shen J. Impact of ultraviolet radiation on HDPE and HDPE/STC blends. Polymers for Advanced Technologies. 2008;20(3):341-6.

[48] Jin ZM, Medley JB, Dowson D. Fluid film lubrication in aritificial hip joints. Tribology and Interface Engineering Series. 2003;41:237-56.

[49] Assouline E, Lustiger A, Barber AH, Cooper CA, Klein E, Wachtel E, Wagner HD. Nucleation ability of multiwall carbon nanotubes in polypropylene composites. Journal of Polymer Science. 2003;41(5):520-7.

[50] Rosca ID, Watari F, Uo M, Akasaka T. Oxidation of multiwalled carbon nanotubes by nitric acid. Carbon. 2005;43(15):3124-31.

VITA

Name:	Fangzhou Feng
Address:	Department of Mechanical Engineering c/o Dr. Hong Liang Texas A&M University College Station, TX 77843-3123
Email Address:	halleyark@yahoo.com.cn fengfz@tamu.edu
Education:	B.S., Mechanical Engineering and Automation, Wuhan University of Technology, China, 2008 M.S., Mechanical Engineering, Texas A&M University, 2010